PERGAMON

Journal of Structural Geology 22 (2000) 647–667

JOURNAL OF STRUCTURAL GEOLOGY

www.elsevier.nl/locate/jstrugeo

Magnetic fabric and deformation in charnockitic igneous rocks of the Bjerkreim–Sokndal layered intrusion (Rogaland, Southwest Norway)

Olivier Bolle[a,*], Hervé Diot[b], Jean-Clair Duchesne[a]

[a]*L.A. Géologie, Pétrologie et Géochimie, Université de Liège, Bd. du Rectorat, B20, B-4000 Sart Tilman, Belgium*
[b]*C.L.D.G., Pôle Sciences et Technologie, Université de La Rochelle, Av. Marillac, F-17042 La Rochelle Cedex 01, France*

Received 2 December 1998; accepted 3 December 1999

Abstract

The Bjerkreim–Sokndal intrusion (BKSK) belongs to the Proterozoic Rogaland igneous complex of Southwest Norway. The BKSK displays an anorthosite to mangerite cumulate series, folded into a syncline, in the core of which crop out massive acidic rocks of quartz mangerite to charnockite composition. We present a study which focuses on the acidic rocks, in which we use the low-field anisotropy of magnetic susceptibility (AMS) technique. Systematic microscope examination of the samples collected at 148 AMS stations, and considerations based on mineral intrinsic magnetic susceptibilities reveal magnetic mineralogy and anisotropy controlled by magnetite. Macro- to micro-scale petrofabrics and magnetic fabrics indicate that the acidic rocks, which intruded after deposition of the underlying cumulate series, were also affected by the syn- to post-magmatic folding event which gave rise to the BKSK syncline. In absence of any recognized plate-scale regional stress field, it is suggested that this folding results from a gravity-induced subsidence linked to the final stage of diapiric emplacement of huge neighbouring anorthosite plutons. This model is mainly supported by the structural pattern in the BKSK, which reveals a convergent flow towards a central trough where lineations are sub-vertical.

1. Introduction

The Bjerkreim–Sokndal intrusion (BKSK) (Michot, 1960; Wilson et al., 1996; Duchesne and Wilmart, 1997) is a layered magmatic body belonging to the Proterozoic Rogaland igneous complex of Southwest Norway. It is a well-documented case of magmatic complex of the AMCG suite (anorthosite–mangerite–charnockite–(rapakivi) granite)[1]. The BKSK displays a layered lower part of cumulative origin, here called the cumulate series, and an upper part made up of massive quartz mangerite and charnockite, here called acidic rocks. This magma chamber, flanked by anorthosite plutons, is folded. Field and petrological evidence (Duchesne et al., 1985; Duchesne and Maquil, 1987), and a recent numerical modelling (Barnichon et al., 1999) have shown that diapirism is a robust and consistent mechanical hypothesis for the emplacement of these anorthosite bodies. A previous micro- to macro-scale structural study, conducted on a restricted portion of the cumulate series (Paludan et al., 1994), also suggests that the BKSK has been affected by a gravity-induced subsidence, coeval with the diapirism of the neighbouring anorthosite plutons.

This paper reports the results of a BKSK survey, using the low-field anisotropy of magnetic susceptibility (AMS) technique (e.g. Rochette et al., 1992; Borradaile and Henry, 1997), which allows rapid and

* Corresponding author. "Chargé de Recherches du Fonds National Belge de la Recherche Scientifique".
E-mail address: obolle@ulg.ac.be (O. Bolle).

[1] Nomenclature of the AMCG rocks used in the present paper is as follows (Streckeisen, 1974): anorthosite = rock containing more than 90% of plagioclase; (leuco)norite = hypersthene (leuco)gabbro; jotunite (or monzonorite) = hypersthene monzogabbro; (quartz) mangerite = hypersthene (quartz) monzonite; charnockite = hypersthene granite.

0191-8141/00/$ - see front matter
PII: S0191-8141(99)00183-2

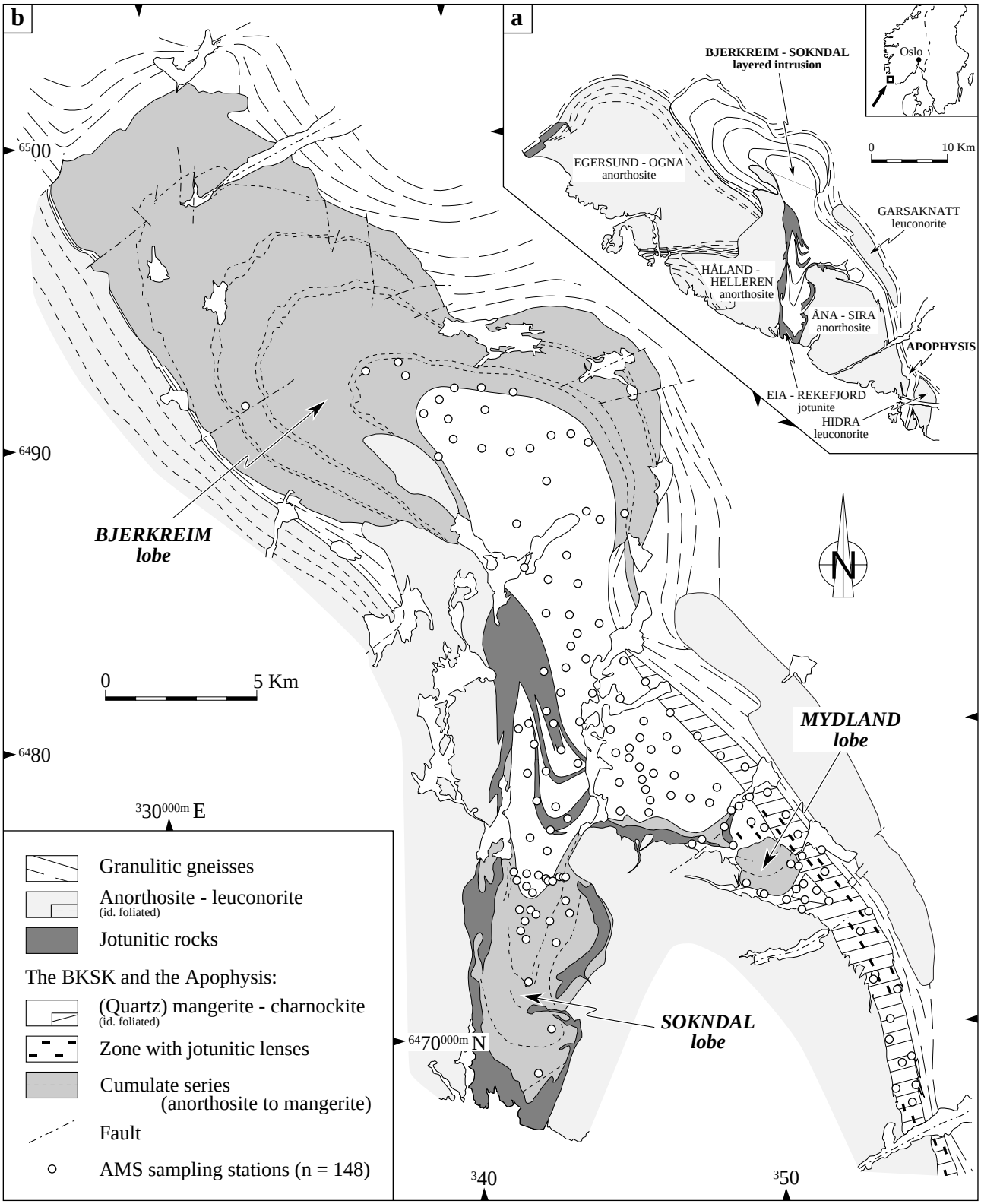

Fig. 1. Geological sketch map of (a) the Rogaland igneous complex; and (b) the BKSK and the Apophysis northern part (after Michot and Michot, 1969; Rietmeijer, 1979; Falkum, 1982; Krause et al., 1985; Duchesne and Maquil, 1987; Wilson et al., 1996; Bolle, 1998). In (a), lithology of the BKSK and the Apophysis is not detailed. In (b), dotted lines in the cumulate series figure the igneous layering and major lithological boundaries (in the Bjerkreim lobe, the stratigraphically lowest dotted line corresponds to the upper limit of major anorthosite occurrence; in the Bjerkreim and Sokndal lobes, the stratigraphically highest dotted line corresponds to the lower limit of the mangerite cumulates). Grid is the EURF89 kilometric UTM grid (32V zone, LK 100 km square).

easy fabric characterization of weakly anisotropic rocks (e.g. Bouchez, 1997). The internal structure of the massive acidic rocks which cap the cumulate series has been pictured. The study, which also deals with petrofabric interpretation at micro- to macro-scales, brings new arguments in favour of a gravity-induced subsidence of the BKSK.

2. The Rogaland igneous complex

2.1. Description

The BKSK (Fig. 1a and b) (Michot, 1960; Wilson et al., 1996; Duchesne and Wilmart, 1997) occupies an area of ~230 km^2. Its cumulate series is folded into a syncline, which branches into three lobes: a major one (the north-western Bjerkreim lobe) and two minor ones (the southern Sokndal and south-eastern Mydland lobes). The axes of these lobes plunge towards the core of the structure, which is occupied by the acidic rocks. The Bjerkreim lobe displays the most complete rock sequence in the cumulate series, more than 7000 m thick in the axial zone of the syncline. The acidic rocks lying above these cumulates are much thinner (< 2000–2500 m). The lowest rocks of the magma chamber crop out in the north-western part of the Bjerkreim lobe, whereas the country rock roof, capping the acidic rocks, has been completely eroded. The acidic rocks extend south-eastward in a thin sheet-like intrusion (Fig. 1a and b), called the Apophysis (Demaiffe, 1972; Bolle, 1996, 1998). This intrusion is a composite magmatic body, made up of acidic and jotunitic rocks.

Beside the BKSK, the main units of the Rogaland igneous complex are three large anorthosite plutons (the Egersund–Ogna, Håland–Helleren and Åna–Sira bodies) (Fig. 1a). The Egersund–Ogna body (Michot, 1960; Duchesne and Maquil, 1987) is dome-shaped and shows a 1–3-km-thick inner margin of foliated anorthosite–leuconorite and an anorthositic central part. The Håland–Helleren body (Michot, 1961) is made up of a foliated and folded anorthosite–leuconorite (the Håland pluton, similar to the Egersund–Ogna margin) and of a massive anorthosite (the Helleren pluton, cutting across the Egersund–Ogna margin and the Håland pluton). Similar to the Egersund–Ogna body, the Åna–Sira anorthosite pluton is dome-shaped, but without foliated margin (Krause and Pedall, 1980; Krause et al., 1985).

Two small leuconoritic intrusions crop out in the country rocks, along the eastern margin of the Rogaland igneous complex: the Garsaknatt and Hidra bodies (Michot and Michot, 1969; Demaiffe et al., 1973; Demaiffe, 1977) (Fig. 1a). Other minor components of the Rogaland igneous complex are rocks of the jotunitic kindred, cutting across the anorthosite plutons and the cumulate series, and forming dykes and small plutons (Duchesne et al., 1989). Among these jotunitic occurrences, the largest body is the Eia–Rekefjord intrusion (Michot, 1960; Wiebe, 1984), which emplaced along the contact between the BKSK and the Helleren and Åna–Sira anorthosites (Fig. 1a and b).

Zircon and baddeleyite U–Pb ages, and whole rock Rb–Sr ages, obtained on various units of the Rogaland igneous complex, indicate an emplacement around 930 Ma, in a very short time interval (Schärer et al., 1996 and references therein).

2.2. Geological setting

The Rogaland igneous complex belongs to the Proterozoic Sveconorwegian/Grenvillian orogenic belt. It was emplaced in high-grade terrains, mainly made up of various ortho- and paragneiss complexes (e.g. Falkum and Petersen, 1980). The country rocks show a metamorphic gradient, from granulite-facies in the surroundings of the complex to amphibolite-facies further east, due to the cumulative effect of three metamorphic events (M_1, M_2, M_3; Maijer, 1987). The most intense event, M_2, is characterized by HT–LP undeformed mineral associations, and results from contact metamorphism induced by the intrusion of the Rogaland igneous complex (Bingen and van Breemen, 1998), at around 5.5 kbar and 800–850°C, as defined by osumilite occurrence close to the contact (Holland et al., 1996).

In agreement with previous works (Michot, 1960; Hermans et al., 1975; and references in Maijer, 1987), Falkum (1998) has described six successive folding phases (F_1–F_6) to the east of the Rogaland igneous complex. F_1 corresponds to intrafolial mesoscopic isoclinal folds. F_2–F_5 have produced folds with dominant N–S fold axes, gradually more tilted axial planes, and decreasing amplitude (from pluri-kilometric-scale recumbent isoclinal folds to small-scale tight folds). F_6 has led to large-scale, open to gentle folds with E–W axes and vertical axial planes. While the F_1–F_5 events are coeval with regional metamorphism, F_6 occurred with only weak recrystallization. The F_1–F_6 detailed chronology and correlation with the M_1, M_2, M_3 metamorphic phases of Maijer (1987) are still uncertain. The last regional-scale folding (F_5) is, however, considered to be 50–60 My older than the emplacement of the ~930 Ma old Rogaland igneous complex (Schärer et al., 1996; Falkum, 1998).

3. Petrology

The AMS sampling has been performed at 148

Table 1
AMS data. *X, Y* = coordinates of the AMS sampling stations in the EURF89 kilometric UTM grid (32V zone, LK 100 km square). In the petrography column, a brief petrographic description of the AMS samples is given (2Px = two-pyroxene acidic rock; Ol = fayalitic olivine–clinopyroxene acidic rock; my = mylonitic rock; f = fine-grained rock; C = cumulate). MS refers to the microstructure type (0, 1, 2, or 3), as defined in the text. K_m = magnitude of the bulk magnetic susceptibility. P', T = anisotropy degree and shape parameter of Jelinek (1981). K_1, K_3 = azimuth and plunge (in degrees) of the magnetic lineation and the magnetic foliation pole, respectively († indicates disregarded values)

Site	X	Y	Petrography	MS	K_m (10^{-3} SI)	P'	T	K_1	K_3
1	54.2	68.9	Qtz mangerite (2Px)	1	18.0	1.26	0.11	†	†
2	54.2	67.3	Qtz mangerite (2Px)	2	30.7	1.61	0.08	159/61	253/2
3	53.9	71.1	Qtz mangerite (2Px)	3	28.3	1.63	0.07	†	†
4	53.9	71.1	Qtz mangerite (2Px)	2	18.1	1.46	0.03	87/86	248/4
5	51.6	75.8	Qtz mangerite (2Px)	2	23.7	1.68	0.69	130/65	222/1
6	53.7	67.8	Mangerite (2Px)	1	22.2	1.42	0.20	152/62	265/12
7	50.9	74.2	Qtz mangerite (2Px)	1	18.6	1.26	−0.14	333/17	233/32
8	51.7	74.1	Qtz mangerite (2Px)	1	21.7	1.19	−0.03	344/3	252/35
9	52.8	73.1	Qtz mangerite (2Px)	1	16.5	1.46	0.03	155/52	56/7
10	53.0	73.7	Qtz mangerite (2Px)	1	21.4	1.34	0.01	126/60	246/16
11	53.2	71.6	Mafic-rich jotunite	1	31.9	1.35	0.17	152/50	251/6
12	53.1	71.4	Qtz mangerite (2Px)	2	21.0	1.55	0.11	128/57	256/21
13	53.6	70.1	Qtz mangerite (2Px)	2	23.0	1.40	0.34	135/66	256/14
14	53.5	69.4	Qtz mangerite (2Px)	1	23.4	1.42	0.06	146/70	268/11
15	49.6	74.5	Qtz mangerite (2Px, my)	3	38.4	1.49	−0.05	302/9	206/35
16	54.4	67.9	Qtz mangerite (2Px)	2	6.5	1.48	0.10	47/73	260/14
17	53.9	68.6	Qtz mangerite (2Px)	1	26.4	1.47	0.03	15/76	249/7
18	50.9	75.6	Qtz mangerite (2Px, my)	3	17.7	1.74	0.02	312/35	58/22
19	51.7	75.0	Qtz mangerite (2Px)	2	18.0	1.81	0.15	334/50	69/5
20	51.3	74.5	Qtz mangerite (2Px)	0	17.6	1.42	−0.00	320/17	228/4
21	51.0	74.7	Qtz mangerite (2Px)	1	16.1	1.56	0.02	327/37	73/20
22	50.7	74.6	Qtz mangerite (2Px)	2	23.3	1.59	−0.27	345/42	120/39
23	50.8	74.0	Mangerite (2Px)	2	45.2	1.22	0.03	359/45	235/29
24	50.4	74.2	Qtz mangerite (2Px)	2	23.0	1.54	−0.14	319/22	220/23
25	49.7	74.5	Qtz mangerite (2Px, my)	3	16.9	1.44	−0.06	310/2	219/28
26	49.9	77.8	Qtz mangerite (2Px)	2	59.6	1.35	0.05	315/69	59/5
27	49.2	77.6	Mangerite (C)	1	33.6	1.43	−0.19	313/60	92/24
28	48.9	77.4	Jotunite (f)	0	11.7	1.60	−0.19	295/78	92/10
29	48.7	77.2	Qtz mangerite (Ol)	1	38.6	1.29	−0.18	300/61	56/13
30	48.4	76.7	Jotunite (f)	1	61.9	1.69	−0.08	342/79	85/2
31	47.7	76.3	Jotunite (f)	0	88.3	2.06	−0.03	14/31	215/57
32	47.3	76.2	Jotunite (f)	1	42.2	1.51	−0.07	7/47	210/40
33	48.7	76.0	Jotunite	1	41.0	1.35	−0.06	314/46	49/3
34	42.6	82.0	Qtz mangerite (2Px)	0	37.9	1.36	0.23	136/77	264/8
35	43.3	82.1	Qtz mangerite (2Px)	1	17.0	1.31	0.03	157/88	75/0
36	43.6	82.8	Qtz mangerite (2Px)	0	18.1	1.20	0.07	146/82	264/4
37	44.2	81.3	Qtz mangerite (2Px)	0	20.5	1.18	0.39	42/76	246/13
38	43.8	80.3	Qtz mangerite (2Px)	0	13.9	1.22	0.03	296/77	65/8
39	45.9	77.3	Qtz mangerite (Ol)	1	32.8	1.07	0.72	304/3	210/57
40	46.0	77.7	Charnockite (Ol)	0	23.3	1.06	−0.35	354/58	189/31
41	45.8	78.1	Charnockite (Ol)	0	8.7	1.09	−0.60	50/76	204/13
42	45.7	78.4	Charnockite (Ol)	0	8.6	1.11	−0.25	104/80	193/1
43	45.7	78.8	Charnockite (2Px)	0	17.4	1.09	−0.09	121/75	212/3
44	45.3	79.1	Charnockite (Ol)	0	9.9	1.11	0.12	140/73	44/2
45	45.3	79.4	Charnockite (2Px)	1	13.1	1.12	0.29	69/79	219/10
46	45.7	79.8	Charnockite (Ol)	0	8.7	1.13	0.30	355/71	234/10
47	45.9	80.3	Charnockite (2Px)	0	35.7	1.15	0.19	119/83	245/5
48	44.8	80.1	Qtz mangerite (Ol)	0	18.8	1.11	0.09	338/54	242/5
49	44.9	79.3	Charnockite (2Px)	0	12.9	1.11	0.11	145/74	46/3
50	44.9	78.3	Charnockite (2Px)	1	8.5	1.09	−0.29	58/80	218/10
51	44.9	77.4	Qtz mangerite (Ol)	1	12.6	1.11	−0.07	352/78	217/6
52	44.7	87.0	Qtz mangerite (Ol)	0	10.7	1.12	−0.27	179/77	278/2
53	44.2	87.3	Qtz mangerite (2Px)	0	11.0	1.15	−0.10	157/66	262/6
54	45.5	87.2	Jotunite (C)	2	45.9	1.48	−0.13	227/73	82/14
55	43.5	85.9	Qtz mangerite (2Px)	0	33.6	1.20	−0.23	193/65	85/9

56	50.8	76.3	Qtz mangerite (2Px)	2	28.9	1.30	0.11	304/48	40/6
57	50.5	77.0	Qtz mangerite (2Px)	1	62.3	1.30	−0.06	308/39	208/12
58	49.7	76.6	Mafic-rich jotunite	1	41.9	1.22	−0.09	288/66	56/15
59	49.3	76.8	Mafic-rich jotunite	1	44.1	1.17	−0.15	303/65	53/9
60	41.5	74.2	Jotunite (C)	2	65.9	1.22	0.05	18/55	272/11
61	42.1	74.0	Mangerite (C)	2	44.2	1.14	0.32	358/45	253/15
62	42.5	73.8	Norite (C)	2	86.0	1.26	0.34	321/37	72/25
63	41.9	74.2	Mangerite (C)	3	44.8	1.16	0.06	356/50	252/12
64	42.7	73.1	Melanorite (C)	1	137.8	1.19	0.49	307/44	90/40
65	43.2	74.0	Melanorite (C)	2	244.0	1.20	0.15	288/33	73/52
66	43.1	74.4	Norite (C)	2	90.6	1.16	0.46	288/41	80/45
67	41.7	80.2	Charnockite (2Px)	0	15.9	1.22	0.04	91/68	253/21
68	42.0	80.4	Charnockite (Ol, f)	0	17.2	1.16	−0.04	80/64	247/27
69	42.6	80.8	Jotunite (f)	0	48.4	1.19	0.08	38/81	238/8
70	43.1	81.3	Qtz mangerite (2Px)	0	12.8	1.14	0.18	32/81	250/7
71	42.9	80.3	Jotunite (f)	1	58.8	1.20	0.07	339/81	248/0
72	43.1	79.5	Mangerite (f)	0	53.9	1.30	−0.30	320/81	57/1
73	43.6	79.0	Qtz mangerite (2Px)	0	35.6	1.16	−0.32	337/79	76/2
74	42.6	78.8	Jotunite (f)	0	75.4	1.20	−0.31	30/60	228/29
75	42.2	79.7	Qtz mangerite (2Px)	0	22.4	1.29	−0.13	94/55	261/35
76	45.3	82.3	Qtz mangerite (Ol)	0	21.1	1.07	−0.36	276/78	54/8
77	46.0	81.6	Charnockite (Ol)	1	12.5	1.17	0.12	10/85	232/4
78	44.5	83.5	Qtz mangerite (Ol)	0	3.6	1.22	0.25	246/79	75/10
79	43.8	83.2	Qtz mangerite (2Px)	0	21.3	1.44	−0.04	304/85	79/3
80	43.9	84.9	Qtz mangerite (2Px)	1	18.4	1.33	−0.04	214/79	85/7
81	42.9	85.1	Qtz mangerite (2Px)	1	13.8	1.19	−0.43	144/81	240/1
82	42.1	85.5	Qtz mangerite (2Px)	0	22.1	1.41	−0.18	143/63	258/12
83	46.7	77.8	Charnockite (Ol)	1	7.2	1.21	−0.11	343/85	199/4
84	47.3	77.7	Charnockite (Ol)	1	9.7	1.35	0.00	54/79	220/11
85	46.8	78.5	Charnockite (Ol)	1	5.5	1.27	−0.05	150/80	43/3
86	46.9	79.3	Charnockite (Ol)	0	6.7	1.25	0.07	138/77	224/1
87	47.6	79.8	Charnockite (Ol)	2	7.4	1.38	0.00	45/83	233/7
88	46.7	80.6	Charnockite (Ol)	0	7.0	1.30	0.11	50/86	225/4
89	46.6	79.8	Charnockite (Ol)	0	9.6	1.32	0.01	126/78	234/4
90	46.1	79.4	Charnockite (Ol)	1	12.9	1.17	0.09	8/78	223/9
91	46.1	78.6	Charnockite (Ol)	1	9.3	1.19	−0.08	120/65	216/3
92	43.1	75.2	Gabbronorite (C)	2	90.0	1.19	0.22	291/48	77/37
93	43.0	75.2	Jotunite (C)	2	26.4	1.28	0.30	335/23	80/31
94	42.9	75.2	Mangerite (C)	2	22.6	1.29	0.08	5/41	97/4
95	42.7	75.1	Mangerite (C)	0	23.1	1.09	−0.06	336/21	85/42
96	42.5	75.1	Jotunite (f)	1	21.9	1.22	0.08	2/44	101/9
97	42.4	75.2	Qtz mangerite (Ol)	0	15.3	1.31	0.08	22/88	272/1
98	42.2	75.3	Qtz mangerite (Ol)	1	13.4	1.14	−0.15	11/49	274/7
99	41.8	75.4	Qtz mangerite (Ol)	1	18.8	1.16	−0.02	19/42	273/17
100	41.4	75.5	Mangerite (C)	0	18.5	1.20	−0.06	329/87	247/5
101	41.5	75.2	Qtz mangerite (Ol)	0	11.9	1.31	−0.19	49/59	264/26
102	41.8	75.0	Qtz mangerite (Ol)	0	13.5	1.25	−0.14	33/59	270/19
103	42.0	74.8	Qtz mangerite (Ol)	0	20.5	1.26	0.11	13/77	266/5
104	41.7	73.8	Mangerite (C)	1	19.2	1.33	0.15	15/57	232/28
105	41.5	73.5	Mangerite (C)	2	31.7	1.24	0.16	359/42	245/24
106	41.7	73.2	Mangerite (C)	0	25.6	1.20	0.13	18/50	248/30
107	41.7	71.8	Jotunite (C)	1	37.1	1.24	0.26	349/6	257/12
108	42.5	70.2	Melanorite (C)	1	190.4	1.24	0.47	20/48	202/43
109	41.9	68.8	Leuconorite (C)	0	1.6	1.10	0.15	14/27	145/52
110	44.4	89.6	Qtz mangerite (Ol)	0	5.7	1.22	−0.21	140/78	43/1
111	43.9	89.9	Qtz mangerite (Ol)	0	2.9	1.37	−0.05	138/84	47/1
112	43.2	89.9	Charnockite (Ol)	1	7.9	1.16	−0.01	138/85	234/1
113	42.5	89.4	Charnockite (Ol)	1	10.3	1.23	−0.01	135/63	234/5
114	41.8	89.4	Charnockite (2Px)	1	6.9	1.16	−0.12	144/54	50/2
115	40.9	89.5	Qtz mangerite (Ol)	1	7.3	1.23	−0.10	139/65	232/2
116	40.0	89.8	Qtz mangerite (2Px)	0	3.7	1.22	−0.25	149/67	245/3
117	39.5	89.4	Qtz mangerite (2Px)	0	14.9	1.25	−0.04	178/62	66/12
118	41.9	78.7	Jotunite (f)	0	41.0	1.43	−0.08	72/64	259/26
119	42.2	77.8	Jotunite (f)	0	29.3	1.29	−0.17	19/57	234/28
120	42.9	77.4	Jotunite (f)	0	28.3	1.29	−0.15	342/54	232/14
121	43.2	77.2	Charnockite (Ol)	0	17.9	1.15	−0.14	70/66	260/23

(continued on next page)

Table 1 (*continued*)

Site	X	Y	Petrography	MS	K_m (10^{-3} SI)	P'	T	K_1	K_3
122	42.7	76.8	Charnockite (Ol)	1	8.3	1.20	−0.24	14/43	234/40
123	42.0	76.6	Charnockite (Ol)	0	5.3	1.21	−0.15	20/76	240/9
124	42.5	76.1	Charnockite (Ol)	0	24.0	1.16	−0.76	14/64	237/21
125	49.2	78.7	Qtz mangerite (2Px, my)	3	38.9	1.55	−0.00	297/75	65/10
126	48.3	79.1	Qtz mangerite (Ol)	1	7.8	1.39	−0.04	288/85	50/3
127	48.2	78.0	Charnockite (Ol)	0	8.7	1.33	−0.16	321/78	54/1
128	47.9	77.5	Charnockite (2Px)	0	19.5	1.41	−0.25	4/65	247/12
129	42.0	91.3	Qtz mangerite (2Px)	0	12.9	1.22	−0.22	129/69	36/0
130	41.1	90.8	Charnockite (2Px)	0	14.4	1.24	−0.17	145/75	248/5
131	41.0	91.6	Qtz mangerite (2Px)	1	6.8	1.34	−0.09	176/76	37/11
132	40.1	91.5	Qtz mangerite (Ol)	0	9.1	1.27	−0.21	140/64	253/10
133	39.6	91.2	Qtz mangerite (Ol)	0	10.8	1.33	−0.22	114/62	217/6
134	39.8	90.5	Qtz mangerite (Ol)	1	8.7	1.20	−0.11	153/60	244/0
135	39.0	90.7	Qtz mangerite (Ol)	1	9.7	1.36	−0.32	127/68	4/13
136	38.5	92.0	Jotunite (C)	2	40.6	1.29	0.29	110/60	211/6
137	37.2	92.2	Jotunite (C)	3	35.7	1.35	0.13	139/53	31/13
138	38.3	92.5	Jotunite (C)	3	16.6	1.39	0.20	131/25	39/5
139	44.0	82.4	Charnockite (2Px)	0	10.8	1.18	0.13	23/84	255/4
140	42.8	84.0	Qtz mangerite (2Px)	0	14.8	1.20	−0.12	15/85	268/2
141	43.5	83.9	Qtz mangerite (2Px)	0	30.2	1.38	0.02	208/83	85/4
142	41.9	86.9	Qtz mangerite (2Px)	1	22.9	1.27	−0.23	152/61	56/3
143	43.0	88.3	Charnockite (Ol)	0	8.9	1.13	−0.45	151/57	251/6
144	45.0	81.1	Charnockite (2Px)	0	18.1	1.15	0.54	299/80	62/5
145	50.6	75.4	Norite (C)	3	41.5	1.35	0.16	332/47	91/25
146	49.0	74.8	Norite (C)	3	59.2	1.31	0.09	91/75	186/2
147	50.9	75.3	Leuconorite (C)	3	5.2	1.06	0.77	19/25	116/12
148	32.9	91.3	Norite (C)	3	124.4	1.35	0.10	103/32	221/36

stations, mainly located in the acidic rocks (Fig. 1b; Table 1). Some samples were also collected in the stratigraphically highest units of the underlying cumulate series, as well as in the northern part of the Apophysis and in the Eia–Rekefjord intrusion.

In the Bjerkreim lobe (Wilson et al., 1996), the cumulate series consists of recurrent megacyclic units made up of andesine anorthosite, leuconorite, norite, gabbronorite (here called the anorthosite–norite cumulates), which pass into jotunite and mangerite rocks (here called the mangerite cumulates) (Fig. 1b). In the Sokndal lobe (Nielsen et al., 1996; Duchesne and Wilmart, 1997), as well as in the Mydland lobe (Schiellerup, personal communication, 1997), only the highest units of the cumulate series are observed, i.e. the mangerite cumulates and the top of the anorthosite–norite cumulates.

The acidic rocks of the BKSK (Duchesne and Wilmart, 1997) and those of the Apophysis (Bolle, 1996, 1998) mainly consist of quartz mangerite and charnockite. In the Apophysis northern part, mafic-rich jotunitic lenses (up to 200 m thick), considered as magma pockets laden with mafic minerals, are interleaved with this acidic material (Bolle, 1998). In the Eia–Rekefjord intrusion, the southern and south-eastern areas are jotunitic in composition, while a continuum from jotunite to mangerite is observed in the northern area (Wiebe, 1984).

The rocks are medium- to coarse-grained (feldspars up to 10 mm long, locally up to 10 cm in the lowest units of the anorthosite–norite cumulates of the Bjerkreim lobe; Wilson et al., 1996; Duchesne and Wilmart, 1997; Bolle, 1996, 1998), except in the Eia–Rekefjord intrusion where finer-grained textures are the rule (Michot, 1960; Wiebe, 1984). The mineralogy is monotonous: the rocks contain, in variable amounts according to their petrography, (antiperthitic) plagioclase, mesoperthitic and/or (micro)perthitic potassium feldspar, quartz, primary orthopyroxene or inverted pigeonite, and clinopyroxene. Fe-rich olivine is present from the mangerite cumulates upwards into the acidic rocks, where two rock types, intimately associated in the field, are observed: a fayalitic olivine–clinopyroxene type and a two-pyroxene type (the acidic material of the Apophysis is petrographically similar to this latter type). Ilmenite, magnetite, apatite, ferro-edenitic hornblende, biotite, and scarce zircon are accessory minerals.

Major and trace element geochemistry and field evidence indicate that the acidic rocks, the apophysis and the Eia–Rekefjord intrusion were emplaced after solidification of the cumulate series as concomitant

mingled/mixed magma batches (Wiebe, 1984; Duchesne and Wilmart, 1997; Bolle, 1998). Note particularly that, in the Mydland lobe, the acidic rocks and the coeval apophysis material have brecciated the cumulate series, which forms a large circular enclave (the Mydland enclave; Bolle et al., 1997) (Fig. 1b).

Experimental studies on the parental magma of the cumulate series indicate P–T crystallization conditions ≤ 5 kbar and 1150–1090°C (Vander Auwera and Longhi, 1994). The liquidus temperature of the acidic rocks is estimated at around 900°C (apatite–zircon saturation temperatures; Duchesne and Wilmart, 1997) and the solidus temperature is ~850–800°C (orthopyroxene–clinopyroxene geothermometer; Wilmart and Duchesne, 1987).

4. Petrofabrics

4.1. Structures in the acidic rocks

Penetrative mesoscopic-scale foliation and lineation can be observed in the acidic rocks and in the concomitant Apophysis and Eia–Rekefjord intrusion. This L/S fabric is defined by a shape-preferred orientation of the rock-forming minerals, namely potassium feldspar ovoids in the acidic rocks, and by elongated, interstitial aggregates of mafic minerals. It is also defined by the alignment of country rock xenoliths, ellipsoidal microgranular enclaves and, especially in the Apophysis, of thin and continuous mafic mineral aggregates. The foliation is generally roughly defined and measurable only in terms of strike. It is however better expressed (Figs. 1b and 2a) in the Apophysis (Bolle et al., 1997) and in a zone developed in the acidic rocks, along the eastern margin of the BKSK, first described by Rietmeijer (1979) and called here the north-western extension of the Apophysis. The intensity of the lineation varies concordantly with that of the foliation, and both variations are very progressive.

The magmatic versus tectonic nature of the L/S fabric has been constrained by a systematic microstructural study of thin sections made from the AMS samples. In the acidic rocks of the BKSK and the

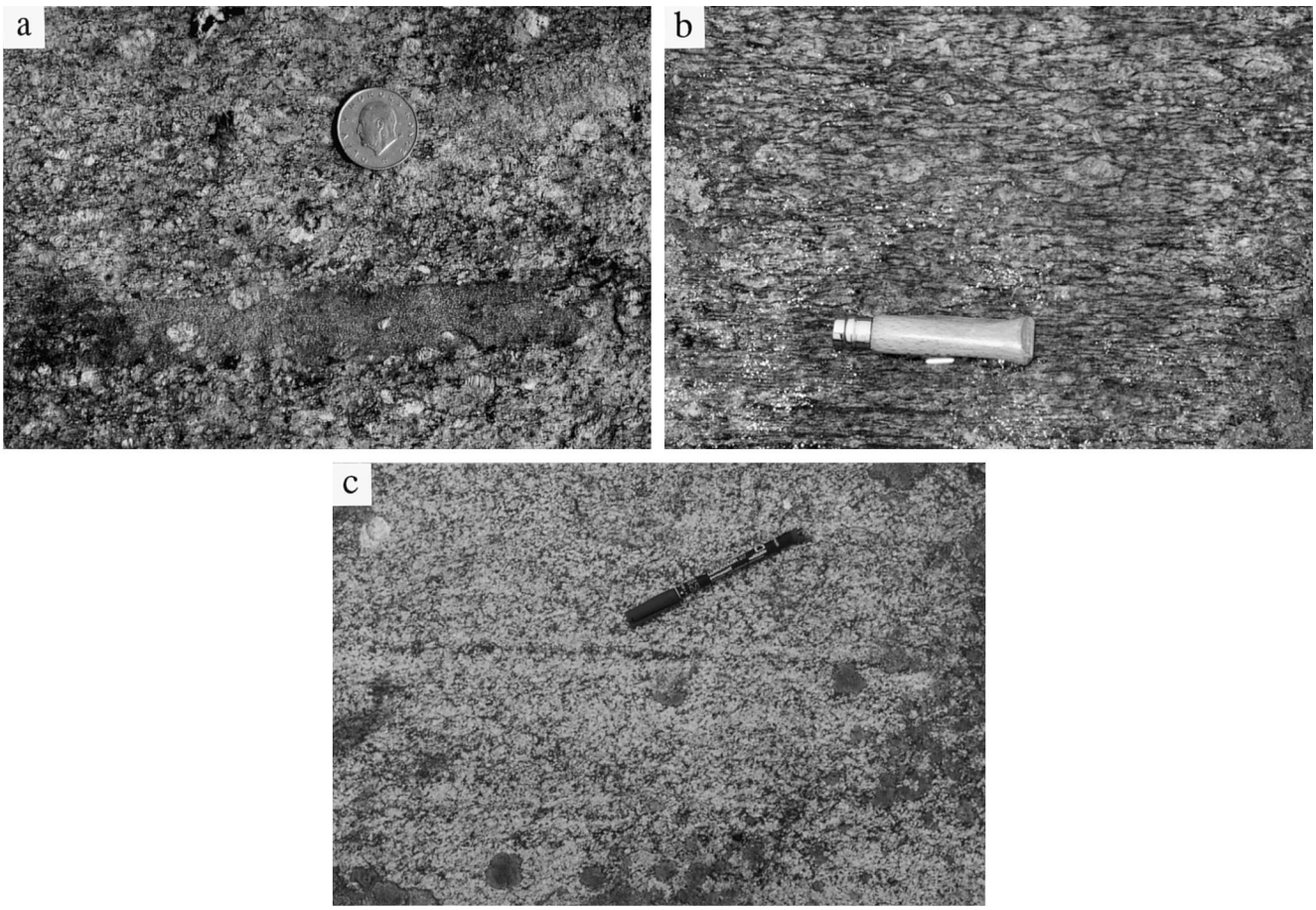

Fig. 2. Field photographs. (a) Foliated quartz mangerite from the Apophysis. Note the shape-preferred orientation of potassium feldspar ovoids and the elongated aspect of a mafic microgranular enclave; (b) Mylonitized quartz mangerite from the Apophysis, near the eastern contact of the Mydland enclave; (c) Norite cumulate showing a compositional layering (S_0) (parallel to the photograph long side) crosscut by an ill-defined, oblique foliation (S_1) (parallel to the pen).

Apophysis, textures are typically of igneous origin but show evidence of various degrees of solid-state deformation. Four types of microstructures have been distinguished, with increasing deformation degree and recrystallization: (1) type 0 (Fig. 3a) is dominantly magmatic, i.e. without substantial solid-state deformation, except limited undulose extinction in quartz or more rarely in feldspar; (2) type 1 (Fig. 3b) displays incipient solid-state deformation characterized by weak dynamic recrystallization of potassium feldspar ovoids, forming ill-defined core-and-mantle textures; (3) type 2 (Fig. 3c) has well-imprinted solid-state deformation features, with well-defined core-and-mantle textures; and (4) type 3 (Fig. 3d) displays a high degree of solid-state deformation and recrystallization, with scarce potassium feldspar porphyroclasts in a matrix of small and elongated grains of feldspars, quartz and mafic minerals.

The latter microstructural classification of the acidic rocks, further extended to all AMS samples, has made it possible to establish the microstructure distribution map shown on Fig. 4. In agreement with the L/S fabric intensity variations observed in the field, this map shows that most acidic rocks still display magmatic fabrics or are incipiently recrystallized, whereas the Apophysis and its north-western extension are more strongly recrystallized (particularly in concordant zones of intense deformation, where mylonitic rocks occur; Fig. 2b).

As a conclusion from the field and microscopic data, the L/S fabric in the acidic rocks underlines a continuum of deformation from magmatic to solid state. In the Apophysis, parallelism of the foliation with thin and continuous mafic mineral aggregates ('schlieren layering' due to magmatic flow sorting, as defined by Irvine, 1987) is complementary evidence (Paterson et al., 1989) in favour of the continuous development of the fabric from magmatic to solid state (Bolle et al., 1997).

4.2. Structures in the cumulate series

A prominent structural feature of the cumulate series is the existence of a planar fabric of igneous origin (S_0) (see e.g. Paludan et al., 1994; Wilson et al., 1996; Duchesne and Wilmart, 1997). This structure is

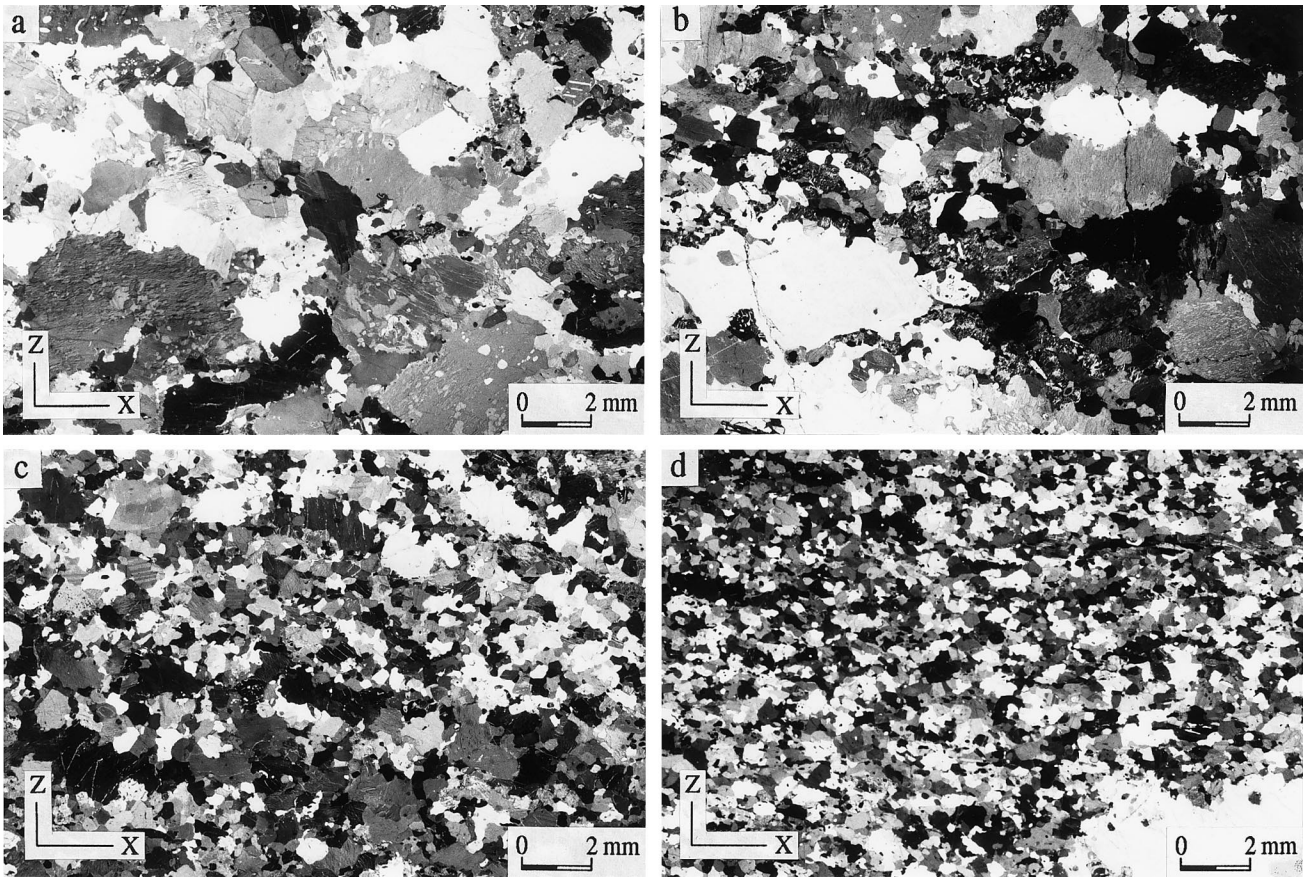

Fig. 3. Microscope photographs (transmitted light, crossed nicols) illustrating microstructures in two-pyroxene acidic rocks. Thin sections are cut parallel to XZ plane (perpendicular to foliation and parallel to lineation). (a) Type 0, dominant magmatic texture (AMS sample 36); (b) Type 1, incipient solid-state deformation (AMS sample 142); (c) Type 2, well-imprinted solid-state deformation (AMS sample 5); (d) Type 3, high degree of solid-state deformation (AMS sample 125). See text for more details.

mainly defined by compositional layering, particularly in the noritic and gabbronoritic rocks. S_0 is also locally expressed by igneous lamination, defined by shape-preferred orientation of euhedral plagioclase crystals in the anorthosite–norite cumulates, or of potassium feldspar ovoids in the mangerite cumulates.

In the Bjerkreim lobe, Paludan et al. (1994) have evidenced a penetrative, mesoscopic-scale, linear and planar tectonic fabric (L_1/S_1), overprinting S_0 in the anorthosite–norite cumulates, and defined by a shape-preferred orientation of individual crystals and aggregates of mafic minerals. These authors have observed a conspicuous increase of this L_1/S_1 fabric intensity, defined both by field evidence and variation of the recrystallization degree, from the lower part of the Bjerkreim lobe hinge zone towards its upper part and the lobe limbs. They have also observed that S_1 is very weak or absent in the hinge zone, the rocks being dominantly L-tectonites (in the sense of Flinn, 1965). Our field (Fig. 2c) and microstructural (Fig. 4) observations unequivocally show that the L_1/S_1 fabric is also present in the mangerite cumulates of the Bjerkreim lobe, and in the whole cumulate series of the Sokndal lobe and the Mydland enclave.

In the Bjerkreim lobe, a progressive increase in thickness of the cumulate layers is observed from the limbs towards the hinge zone (Fig. 1b). This feature has been taken as good evidence that folding of the

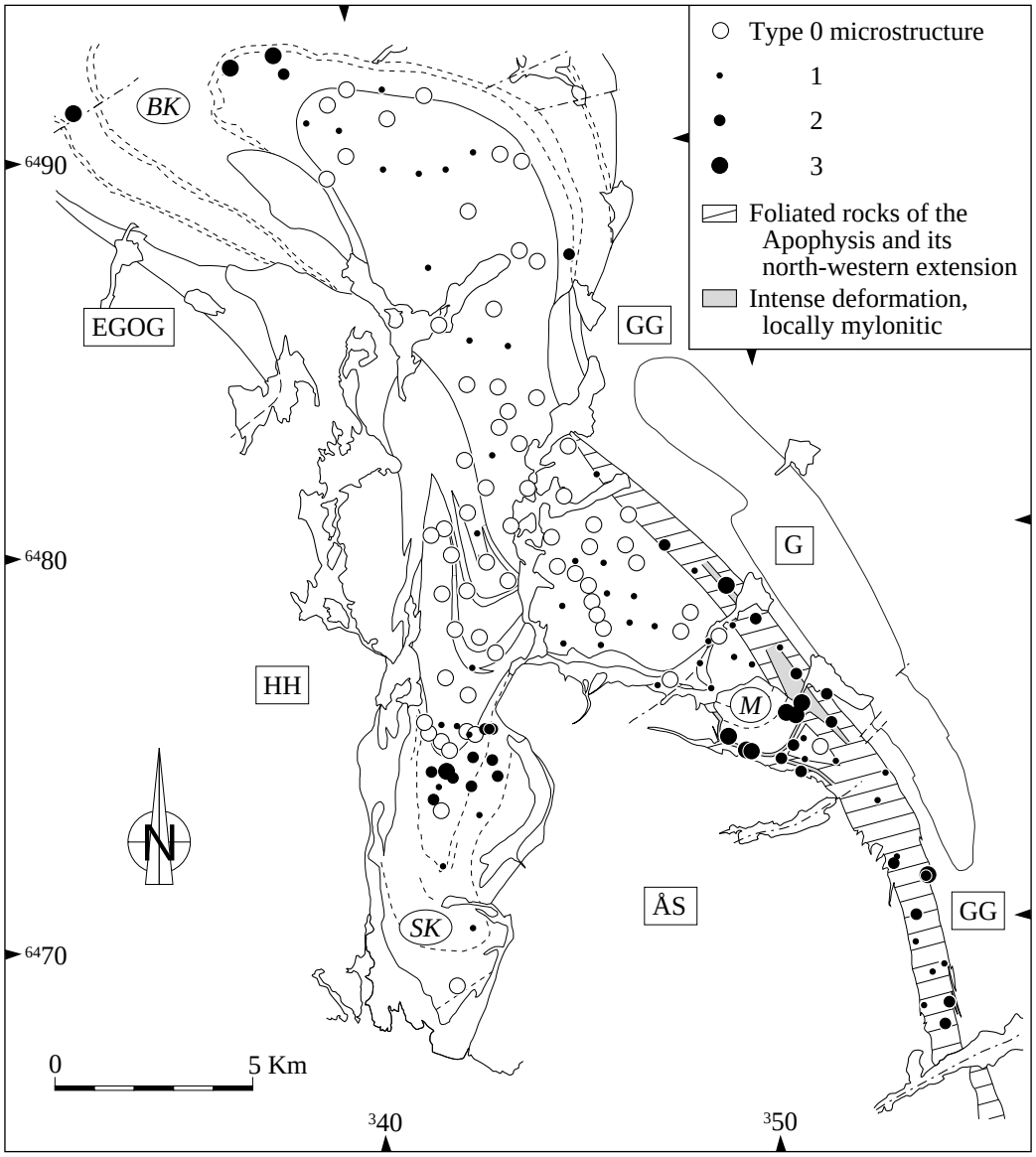

Fig. 4. Distribution map of the microstructures observed in the AMS sample set. BK, SK, and M = Bjerkreim, Sokndal, and Mydland lobes, respectively; EGOG, HH, and ÅS = Egersund–Ogna, Håland–Helleren, and Åna–Sira anorthosite plutons, respectively; G = Garsaknatt leuconorite body; GG = Granulitic gneisses.

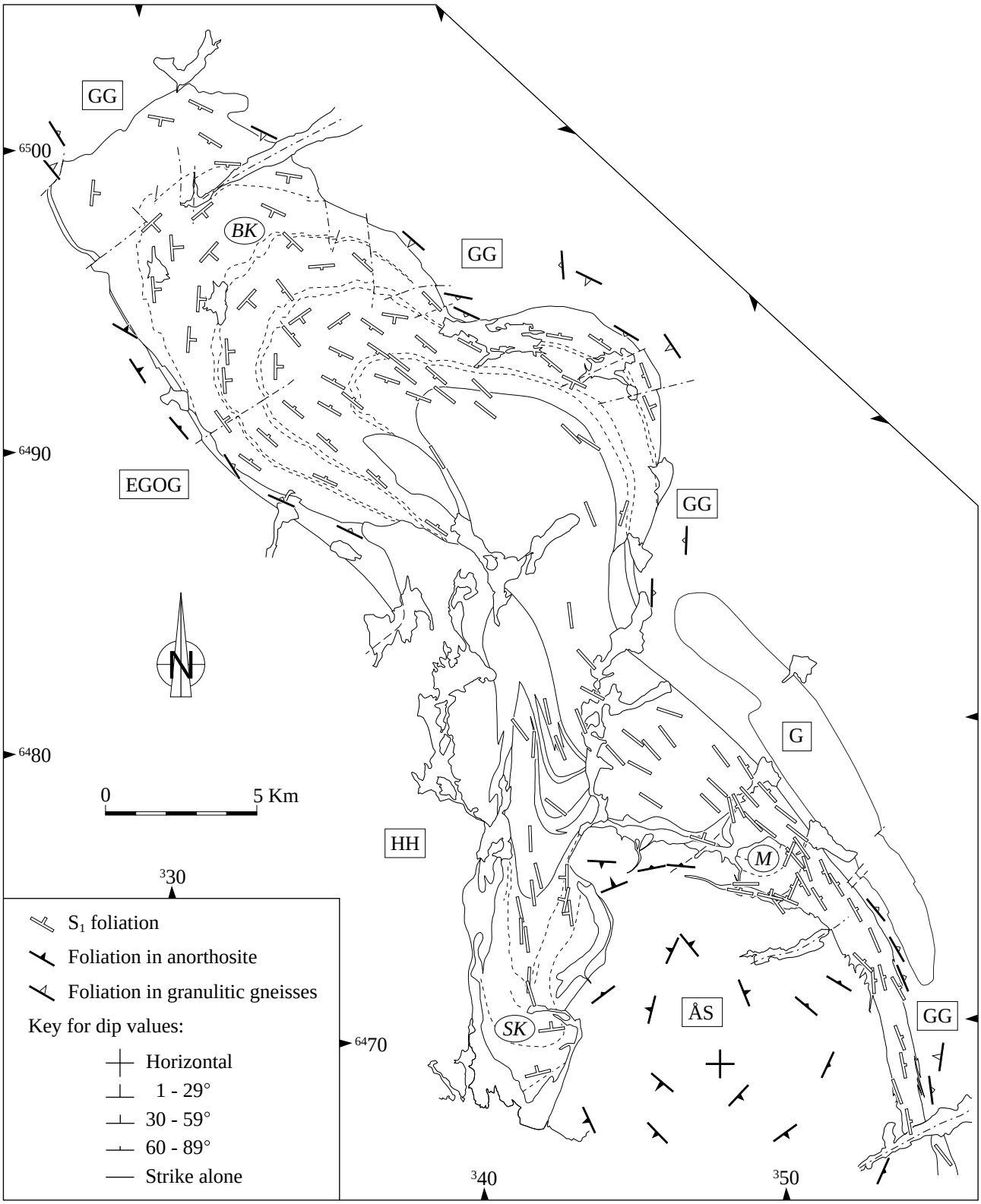

Fig. 5. Field foliation map. Most foliations inside the Bjerkreim lobe are from Paludan et al. (1994). Inside the Åna–Sira anorthosite, foliation measurements are from Krause and Pedall (1980). Foliations in the granulitic country rocks are from Falkum (1982), Paludan et al. (1994), and our own field observations. Acronyms in and around the BKSK are the same as in Fig. 4.

BKSK was already operating during crystallization of the anorthosite–norite cumulates (Michot, 1960; Nielsen and Wilson, 1991). Paludan et al. (1994) further suggested that the increase in the degree of rock recrystallization and intensity of the L_1/S_1 fabrics, from the limbs to the hinge zone of the Bjerkreim lobe, is another indication of syn-magmatic development of the BKSK syncline. Accordingly, the progressive tilting of the magma chamber floor during crystallization of the anorthosite–norite cumulates would have produced a flow of unconsolidated material on the floor. With progressing folding and continuing crystallization, the magmatic flow progressively transformed into a solid-state flow, which superimposed a tectonic foliation onto the igneous lamination of the limbs. The L_1/S_1 fabric observed in the cumulate series is therefore considered to have been acquired continuously from magmatic to solid state.

4.3. Foliation pattern

In the Bjerkreim lobe (Fig. 5) (Michot, 1960; Paludan et al., 1994), the major structure underlined by the S_0 magmatic fabrics and the lithological boundaries is an isoclinal fold, whose N125°E-trending axis plunges ~35° to the south-east. S_0 is sub-vertical in both limbs and locally overturned along the north-eastern contact. In the Sokndal lobe (Fig. 5) (Michot, 1960), the fold axis is north–south in trend and plunges ~40° to the north. In the Mydland enclave (Fig. 5), the layer structure suggests a north-west-plunging fold axis.

As a rule, the S_1 foliation in the cumulate series is parallel to S_0, so that both planar structures define the folding of the BKSK lobes (Fig. 5). Strong obliquities between S_0 and S_1 are, however, locally observed (Figs. 2c and 5): (1) in the upper part of the hinge zone of the Bjerkreim and Sokndal lobes, where S_1 is sub-vertical and parallel to the axial planes; and (2) in the southern part of the Mydland enclave, where S_1 is parallel to the contact with the Apophysis. In the south-western and north-eastern limbs of the Bjerkreim lobe, S_1 is parallel to planar fabrics (mineral foliation and compositional layering) observed in the foliated border of the Egersund–Ogna anorthosite and in the granulitic country rocks, respectively (Fig. 5).

Field observations from the acidic core of the BKSK syncline suggest an ill-defined foliation pattern, striking parallel to the fold axial plane of the Bjerkreim and Sokndal lobes, and branching, east of the Åna–Sira anorthosite, towards the Apophysis (Fig. 5). In the latter body (Bolle et al., 1997), the well-defined foliation is sub-vertical to easterly dipping. It is concordant with both the eastern and western contacts of the intrusion and with the planar fabrics of the granulitic gneisses (Fig. 5). Note that the homogeneous foliation pattern of the Apophysis is disturbed to the south-east of the Mydland enclave: a foliation neutral point can be defined around an area where almost massive acidic rocks occur (Bolle et al., 1997) (Figs. 4 and 5). This neutral point is delimited by zones of intense, locally mylonitic deformation. Its north-western border is concordant with the S_1 foliation that cuts across S_0 in the southern part of the Mydland enclave.

4.4. Preliminary structural interpretation

The few foliation strikes observable in the acidic rocks are concordant with the S_1 fabric that cuts across the cumulate series in the hinge zones of the Bjerkreim and Sokndal lobes (Fig. 5). On this geometrical basis, it is concluded that the acidic rocks were also affected by the folding event that gave rise to the syncline structure and was responsible for the penetrative deformation of the cumulate series. This folding has also produced the concordant inter-fingered folded pattern of Eia–Rekefjord and BKSK material in the Sokndal lobe core (Fig. 1b). It is stressed, however, that the acidic rocks possibly achieved their complete crystallization later in the deformation process, as suggested by the weakness of their L_1/S_1 fabric.

Moreover, existence of a sub-vertical, syn- to post-magmatic shearing along the eastern contact of the Rogaland igneous complex is suggested by: (1) the strong solid-state deformation fabric of the Apophysis and its north-western extension; and (2) the rigid body behaviour played by the Mydland enclave during the deformation, as evidenced namely by the foliation neutral point (Bolle et al., 1997). The shearing at the eastern contact was, at least partly, coeval with the BKSK folding, as suggested by concordance between planar structures in the BKSK acidic rocks and in the

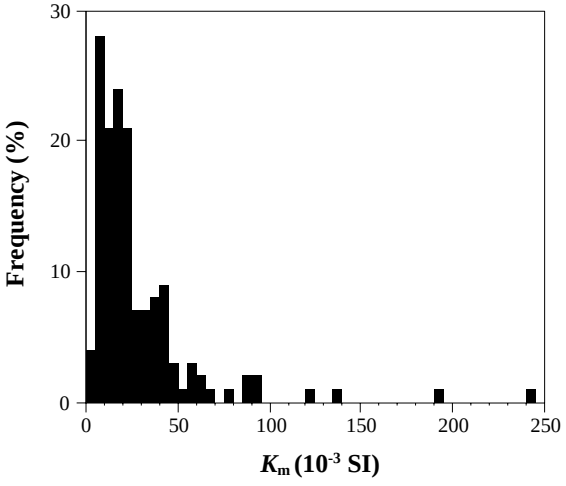

Fig. 6. Histogram of the bulk magnetic susceptibility (K_m) frequency.

Table 2
(a) Magnetic behaviour and intrinsic magnetic susceptibilities of the AMS sample rock-forming minerals. Sources: Borradaile and Henry (1997), Clark (1997). (b) Calculation of ilmenite and magnetite contribution to bulk magnetic susceptibility for samples representative of five BKSK petrographic types. Petrography of these samples is as in Table 1. The modal proportions of ilmenite (Ilm) and magnetite (Mag) grains were obtained by point counting (the 2σ refers to both ilmenite and magnetite proportions and was calculated following Van der Plas and Tobi, 1965). The hematite content of ilmenite (Hem in Ilm) and the ilmenite content of magnetite (Ilm in Mag) were calculated from the oxide chemistry, measured on physically separated grains (Duchesne, 1972). In the five BKSK representative samples, ilmenite is homogeneous and magnetite shows ilmenite intergrowths. The modal proportions of ilmenite and magnetite were therefore corrected considering that TiO_2 in magnetite comes exclusively from its ilmenite intergrowths. Contribution to K due to ilmenite (K_{Ilm}) and magnetite (K_{Mag}) was further calculated using the intrinsic K values of (a). Bulk magnetic susceptibility averages of n similar AMS samples of the present study is given for comparison with $K_{Ilm+Mag}$ ($=K_{Ilm}+K_{Mag}$)

a.

Mineral	Magnetic behaviour	Intrinsic K (10^{-3} SI)
Feldspars, quartz, apatite, zircon	Diamagnetic	~ -0.014 (mean)
Clino- and orthopyroxene, olivine (fayalite), amphibole, biotite	Paramagnetic	~ 2 (mean)
Ilmenite	Paramagnetic	~ 150
Multidomain magnetite	Ferrimagnetic	~ 2800
Pyrrhotite	Ferrimagnetic (if monoclinic)	~ 1500 (if monoclinic)

b.

BKSK representative samples		Oxide grain modal proportions (%)			Oxide chemistry (%)		Oxide corrected modal proportions (%)			Calculated K (10^{-3} SI)			AMS data	
Name	Petrography	Ilm	Mag	2σ	Hem in Ilm	Ilm in Mag	Ilm	Mag	2σ	K_{Ilm}	K_{Mag}	$K_{Ilm+Mag}$	K_m (10^{-3} SI)	n
64.34	Norite (C)	15.8	2.5	0.6	11.3	1.2	15.9	2.5	0.6	23.8 ± 0.8	70.3 ± 15.4	94.1 ± 16.3	125.6	8
66.104	Jotunite (C)	1.8	1.4	0.3	2.4	15.1	2.1	1.2	0.3	3.1 ± 0.5	34.4 ± 8.8	37.5 ± 9.2	38.3	7
TII	Mangerite (C)	1.2	0.9	0.1	2.9	21.3	1.4	0.7	0.1	2.1 ± 0.1	19.0 ± 2.4	21.1 ± 2.5	29.3	9
66.261	Qtz mangerite (Ol)	1.2	0.5	0.1	2.8	24.3	1.3	0.4	0.1	2.0 ± 0.2	11.2 ± 3.9	13.2 ± 4.1	14.0	21
66.87	Charnockite (Ol)	0.8	0.6	0.1	2.6	21.9	1.0	0.5	0.1	1.5 ± 0.1	12.7 ± 1.6	14.1 ± 1.7	10.6	24

Apophysis. It locally continued down to relatively low temperatures and developed mylonitic structures (Gapais, 1989).

5. AMS sampling and measurement procedures

The 148 AMS stations were sampled with a portable drilling machine or, in a few cases, by collecting oriented samples that were re-oriented and core-drilled in the laboratory. At each station, two 25-mm-diameter oriented cores were drilled. The AMS measurements were performed on the upper part of each core (cut into two 23-mm-high cylinders), using a Minisep (Molspin®) spinner susceptometer working in a weak alternative field (7×10^{-4} T, 10 kHz), with a sensitivity of about 5×10^{-7} SI. For each cylinder (four per AMS station), measurement provides the magnitudes of the three principal, mutually orthogonal axes of the AMS ellipsoid ($K_1 \geq K_2 \geq K_3$), as well as their declination and inclination with respect to the specimen frame. For each AMS station, the averages of the principal axis magnitudes and orientations in the geographical frame have been calculated.

6. Magnetic susceptibility and mineralogy

The bulk magnetic susceptibility magnitude is given by the arithmetic mean of the K_1, K_2, K_3 lengths: $K_m = (K_1 + K_2 + K_3)/3$. In the whole set of AMS samples, K_m values range from 1.6 to 244×10^{-3} SI (Table 1), with a mean value of 28.2×10^{-3} SI and a unimodal frequency distribution (Fig. 6).

In order to assess the contribution of each rock-forming mineral to K_m, a microscopic study of thin and polished sections of the AMS samples has been carried out under transmitted/reflected light. The observed minerals are listed in Table 2(a), together with their intrinsic magnetic behaviour and susceptibility. Two high susceptibility minerals, ilmenite and magnetite, are found as ubiquitous accessory minerals in every petrographic type. Ilmenite is homogeneous or, more rarely, contains hematite exsolutions in the less evolved mineral assemblages from the cumulate series. Magnetite usually contains intergrowths of ilmenite lamellae forming cloth or trellis microstructures resulting from complex oxidation–exsolution processes (Duchesne, 1972). The magnetite grain-size is generally ≥ 50 μm and magnetite thus has a dominant multidomain behaviour (according to Clark, 1997, the lower grain-size limit for such behaviour is defined at around 20 μm). Where magnetite and ilmenite grains are in contact, a reaction rim is commonly observed in the magnetite, pointing to readjustment of the oxide composition (Duchesne, 1972). Pyrrhotite, which shows a strong susceptibility when monoclinic (Jover et al., 1989; Clark, 1997), is another accessory mineral. It

forms very sporadic globules, partly epigenized into pyrite. Present only in trace amounts, its contribution to K_m can therefore be neglected, whatever its structure (monoclinic or not).

Ubiquity of magnetite strongly suggests that the bulk magnetic susceptibility is mainly controlled by this mineral. This agrees with the unimodal frequency distribution of K_m, suggesting a magnetic mineralogy dominated by a single mineral (Borradaile and Henry, 1997), and with the high K_m values ($\gg 10^{-3}$ SI), indicative of a ferrimagnetic behaviour (Rochette, 1987). In order to confirm further the dominant role played by magnetite, the respective contributions to bulk magnetic susceptibility of magnetite and ilmenite (the other, quantitatively significant, high magnetic susceptibility mineral) were calculated for samples representative of five BKSK petrographic types (Table 2b). Comparison of the calculated magnetic susceptibilities induced by magnetite and ilmenite with average bulk magnetic susceptibilities of similar AMS samples confirms the major contribution of magnetite to the bulk magnetic susceptibility (Table 2b). The bulk magnetic susceptibility is therefore a good first order indicator of the magnetite content.

Magnetite content is also expressed by a positive correlation observed between K_m and the colour index: the highest K_m values are found in magnetite-rich, melanoritic rocks of the cumulate series, while the lowest ones are observed in magnetite-poor, acidic rocks and leuconorite cumulates (Tables 1 and 2b). A similar relationship between bulk magnetic susceptibility magnitude and colour index has also been observed in some magnetite-bearing granites (e.g. Ferré et al., 1997; Saint Blanquat and Tikoff, 1997).

7. Anisotropy of magnetic susceptibility

Magnetite-dominated magnetic fabrics result mainly from the shape-preferred orientation of the magnetite grains (Uyeda et al., 1963; Grégoire et al., 1998). Distribution anisotropy, in relation with possible magnetic interactions between magnetite grains or clusters of grains, may also play a role (Hargraves et al., 1991). Both origins of anisotropy have to be considered in the present case, because (see below Fig. 8a): (1) individual magnetite grains are frequently unequant in shape, especially in the most deformed rocks; and (2) in many samples, especially in the two-pyroxene acidic rocks, mafic minerals form clusters in which magnetite grains can be less distant than their diameter value.

7.1. Intensity and shape of the magnetic fabric

P' and T parameters of Jelinek (1981) were calculated for the different AMS stations. These parameters are defined by the following expressions:

$$P' = \exp\sqrt{2\left[\left(\ln\frac{K_1}{K_m}\right)^2+\left(\ln\frac{K_2}{K_m}\right)^2+\left(\ln\frac{K_3}{K_m}\right)^2\right]}$$

$$\text{and } T = \frac{2(\ln K_2 - \ln K_3)}{\ln K_1 - \ln K_3} - 1.$$

P' describes the strength, or anisotropy degree, of the magnetic fabric. It varies from $P' = 1$ (isotropic, spherical AMS ellipsoid) to infinity. T is a shape parameter, pointing to a prolate AMS ellipsoid for $-1 \leq T < 0$

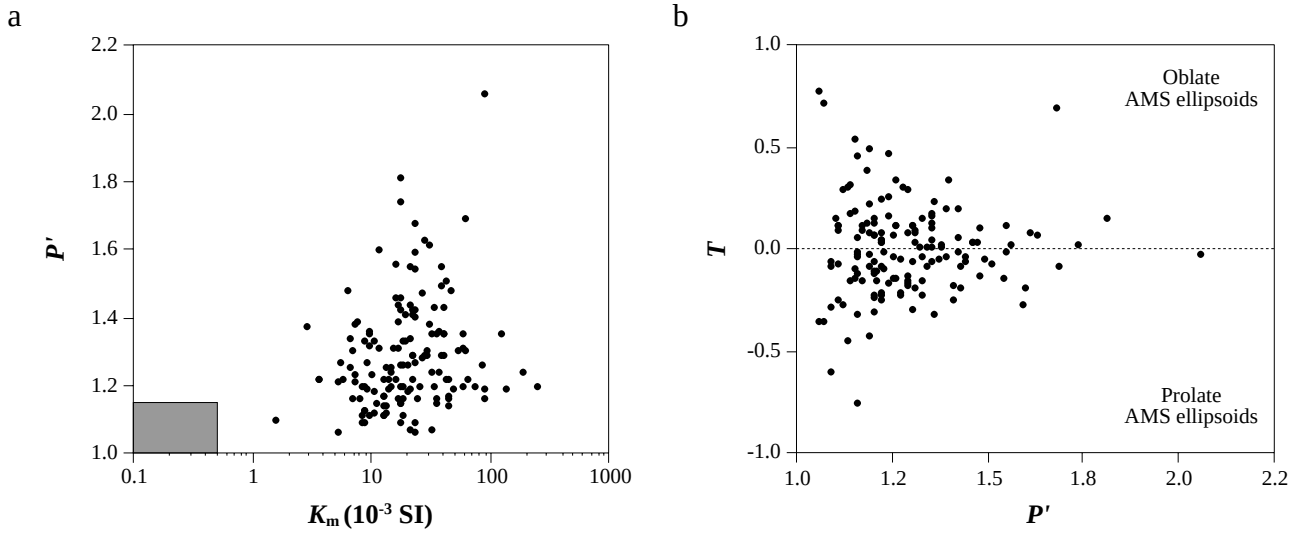

Fig. 7. (a) Variation plot of Jelinek (1981) AMS anisotropy degree (P') vs. bulk magnetic susceptibility (K_m). The shaded area represents the maximum P' and K_m domain of paramagnetic granitoids (after Bouchez, 1997); (b) Variation plot of Jelinek (1981) AMS shape parameter (T) and anisotropy degree (P').

(cigar-shaped for $T=-1$, i.e. $K_2=K_3$), and an oblate ellipsoid for $0 < T \leq 1$ (pancake-shaped for $T = 1$, i.e. $K_1=K_2$).

The value of P' ranges from 1.06 to 2.06 (Table 1), with a mean of 1.29. Some of these values are greater than those reported in the literature for magnetite-bearing granitoids (e.g. Bouchez, 1997; Ferré et al., 1997; Saint Blanquat and Tikoff, 1997; Archanjo et al., 1998). The $P'-K_m$ plot (Fig. 7a) shows that: (1) our data are far outside the domain of paramagnetic granitoids; and (2) there is no obvious correlation between anisotropy degree and magnetic susceptibility magnitude, contrary to what is commonly observed in ferrimagnetic granites (Bouchez, 1997).

T ranges from −0.76 to 0.77 (Table 1), with a zero average value indicating a mean planolinear AMS ellipsoid for the whole sample set. The T–P' plot (Fig. 7b) illustrates the symmetrical disposition of the specimens on both sides of the $T = 0$ line. It further suggests that the AMS ellipsoids tend towards a planolinear shape with increasing anisotropy degree.

A thorough interpretation of these parameters and their variations is beyond the scope of this paper. It would require each petrographic type to be studied separately, in order to take into account the strong mineralogical control on the strength and shape of the magnetic fabric (see Rochette et al., 1992; Borradaile and Henry, 1997).

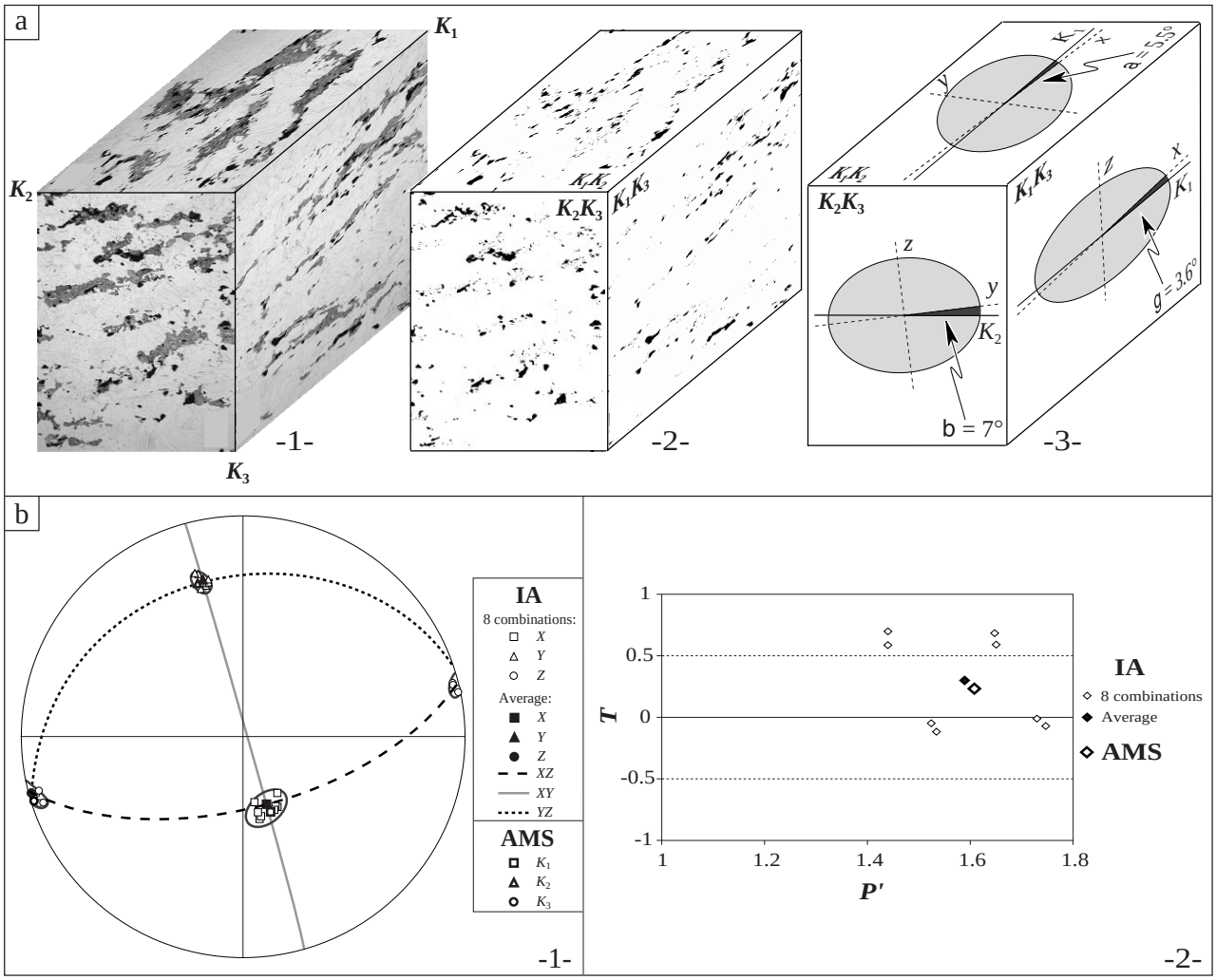

Fig. 8. Image analysis (IA) applied on oxide subfabric (magnetite + ilmenite) of AMS sample 2 (two-pyroxene quartz mangerite from the Apophysis). (a) 3D reconstructed block of three thin sections cut parallel to the K_1K_3, K_1K_2, K_2K_3 planes, respectively. From left to right, for each thin section: (1) microscope natural light view (note shape-preferred orientation and clustering of opaque minerals and Fe-silicates); (2) 2D oxide subfabric, obtained by thresholding of the microscope view; and (3) 2D calculated quadratic shape tensor (Shimamoto and Ikeda, 1976) of the oxide subfabric, obtained by using the inertia tensor program of Launeau and Robin (1996); (b) Comparison of the AMS ellipsoid with the 3D quadratic shape tensor (Shimamoto and Ikeda, 1976) of the oxide subfabric, reconstructed on the basis of 2×3 mutually orthogonal 2D shape tensors (eight combinations) by using the averaging method of Launeau and Cruden (1998). From left to right: (1) Schmidt stereo-plots (lower hemisphere) of the principal axes; and (2) plot of the Jelinek (1981) shape parameters (T) and anisotropy degrees (P').

7.2. Significance of the magnetic fabric orientation

It is commonly assumed that the magnetic lineation (K_1 direction) and magnetic foliation (plane normal to K_3) are parallel to the mineral lineation and foliation, respectively. However, as discussed by Rochette et al. (1992), Borradaile and Henry (1997), and Rochette et al. (1999), this assumption of coaxiality between magnetic fabric and petrofabric is only valid when the following conditions are fulfilled: (1) there are no competing magnetic fabrics; (2) no significant mineralogical source of abnormal magnetic fabrics is present in the rock; and (3) the magnetic fabric has developed in a homogeneously strained domain, within a massive plutonic body for instance. Among these conditions, it is noteworthy that the first one is most certainly fulfilled here, since all rock-forming minerals in the BKSK (including the oxides; Duchesne, 1996) are of igneous origin and have continuously recrystallized, during syn-emplacement deformation, with no change in the mineralogy. Moreover, the subsolidus mineral readjustments have not significantly altered the AMS orientation, since the ilmenite intergrowths and the reaction rims in magnetite grains did not lead to important change in the shape of their host.

Coaxiality between magnetic fabric and petrofabric has been tested for some AMS samples by using the image analysis techniques of Launeau and Robin (1996) and Launeau and Cruden (1998) applied to thin sections cut parallel to the K_1K_2, K_1K_3, K_2K_3 planes. In the example shown on Fig. 8, image analysis demonstrates that the K_1, K_2, K_3 directions are parallel to the corresponding shape principal axes of the oxide subfabric (magnetite + ilmenite): (1) obliquities of less than 10° are observed between the long axes of the 2D quadratic shape tensors and the corresponding magnetic axes (Fig. 8a); and (2) discrepancies, in terms of orientation, shape and strength, between the reconstructed 3D shape tensor and the AMS ellipsoid, are also negligible (Fig. 8b). Since, in addition, a close correspondence between the AMS orientation data and the field measurements is actually observed, as well in the Apophysis (Bolle et al., 1997) as in the whole studied area (see below, Section 7.3), this image analysis study strengthens the fact that magnetic fabric and petrofabric can be equated in the present study.

7.3. Magnetic foliation and lineation

Magnetic foliation and lineation maps are given in Figs. 9 and 10, respectively. On both figures, field directional data have also been reported, including S_1 and L_1 measurements of Paludan et al. (1994) in the Bjerkreim lobe. This combined representation illustrates the parallelism existing between the magnetic orientation data and the planar and linear fabrics measured in the field. In Figs. 9 and 10, the outlines of the Bjerkreim, Sokndal and Mydland lobes are drawn on the basis mainly of the magnetic/L_1 lineation pattern. This cartographic subdivision leads to the definition in the BKSK of a fourth zone, called here the 'central zone', due to its central position with respect to the three lobes.

The magnetic foliation pattern (Fig. 9) agrees with that of S_1, already described in Section 4.3. Its main interest is to emphasize the planar structures within the mostly massive acidic rocks. There, the magnetic/S_1 foliation pattern is very homogeneous in strikes and steeply dipping (e.g. in the central zone, the calculated mean magnetic foliation is N147° NE 87°; Fig. 11a: zone II). Note, however, that where approaching the anorthosite bodies, the foliation strikes are deflected towards parallelism with the contacts. This is obvious in the northern part of the Sokndal lobe and in the north-western part of the Mydland lobe. This is also the case in the limbs of the Bjerkreim and Sokndal lobes where the magnetic/S_1 fabric is parallel to the igneous layering, itself parallel to the flanks of the anorthosite plutons. It is therefore concluded that the planar fabric in the BKSK tends everywhere to wrap around the anorthosite plutons.

Concerning the magnetic/L_1 lineations, Fig. 10 shows that the Bjerkreim and Sokndal lobes have similar patterns. In each lobe, a remarkable convergent pattern of the lineations is evidenced, across all the folded layer boundaries, from the limbs, towards the hinge zone, and finally towards the central zone. In the limbs, the pattern of convergent lineations locally implies strong rotations of the lineation directions. Change of lineation trends are accompanied by variation of the plunge values: in the anorthosite–norite cumulates, plunges are usually gentle to moderate; in the mangerite cumulates and in the acidic core of the lobes, they are moderate to steep; and, in the central zone, they are nearly vertical (calculated mean magnetic lineation at N62° NE 87°; Fig. 11b: zone II). It is noteworthy that: (1) in the limbs of the Bjerkreim lobe, parallelism between the lineations and mineral lineations measured in the granulitic rocks is observed; and (2) in the hinge zone of the Bjerkreim and Sokndal lobes, lineations are roughly parallel to the fold axis.

In the Mydland lobe (Fig. 10), lineations also converge towards the central zone, with increasing plunge values, and cut across the Mydland enclave, except near the contact with the Apophysis where the lineation pattern is perturbed. This further illustrates the interference between the rigid Mydland enclave and the surrounding rocks, already evidenced by the foliation neutral point.

South-east of the Mydland enclave, in the Apophysis (Bolle et al., 1997), the lineation pattern is definitely different from the one observed in the BKSK (Fig. 10):

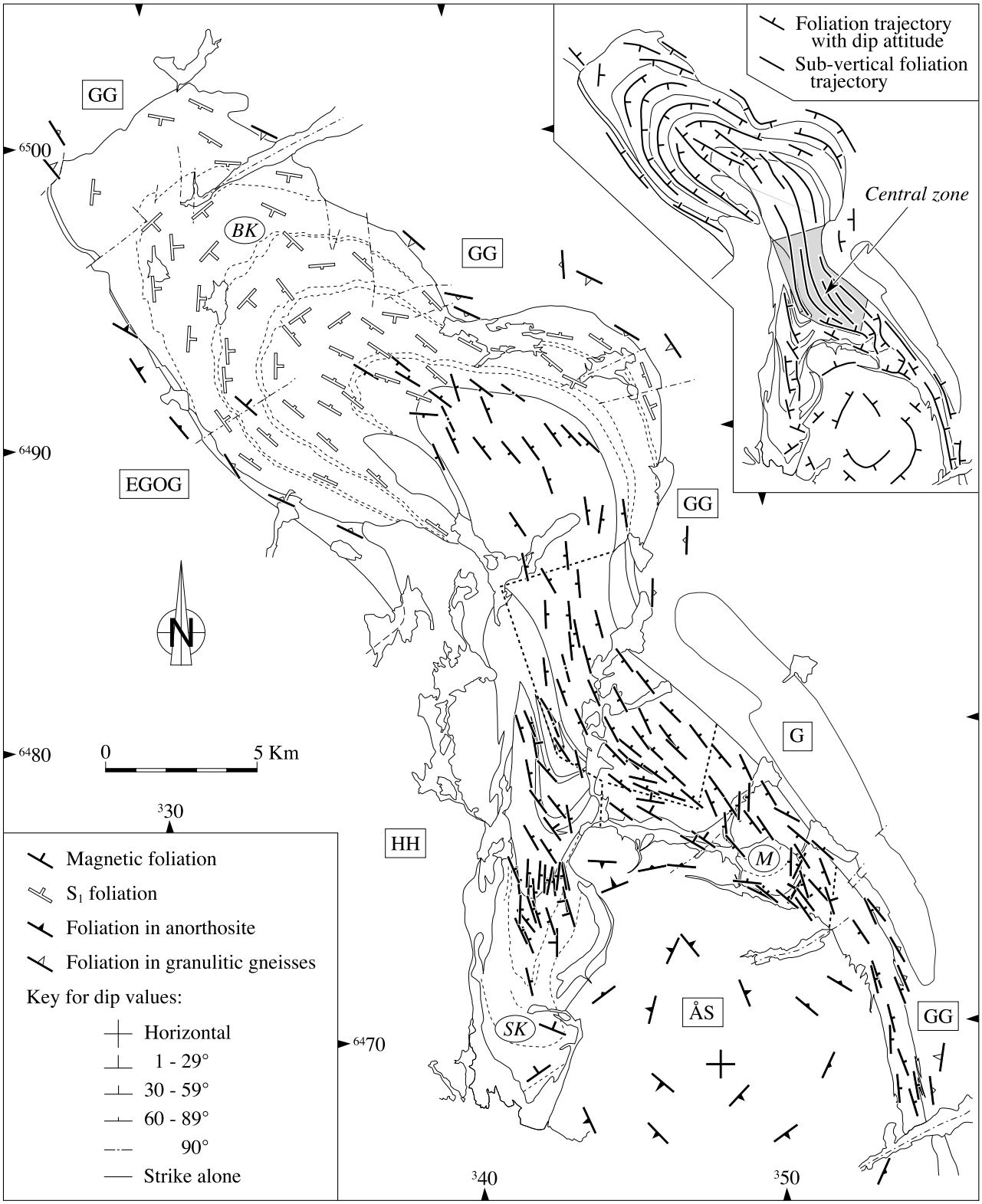

Fig. 9. Magnetic foliation map. The S_1 fabrics measured by Paludan et al. (1994) in the Bjerkreim lobe, and the foliations observed in the granulitic gneisses and in the neighbouring anorthosite plutons (see Fig. 5) are also drawn. The general pattern of these magnetic and S_1 planar structures is synthesized by the foliation trajectories (inset). Acronyms in and around the BKSK are the same as in Fig. 4. Limits of the Bjerkreim, Sokndal, and Mydland lobes (dashed lines) are as defined in the text.

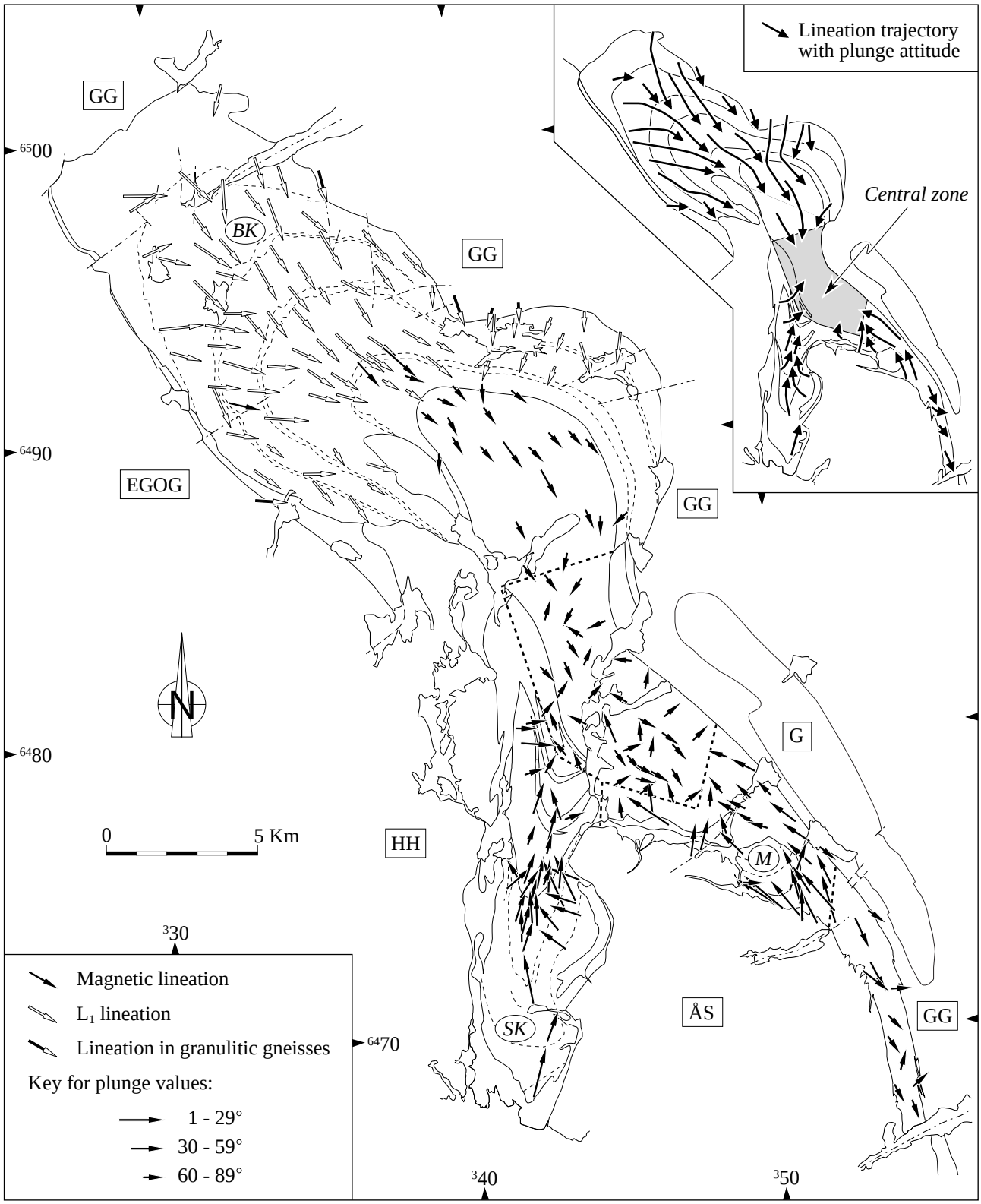

Fig. 10. Magnetic lineation map. L_1 fabrics and mineral lineations measured by Paludan et al. (1994), in the Bjerkreim lobe and in the surrounding granulitic gneisses, respectively, are also drawn. The general pattern of these magnetic and L_1 linear structures is synthesized by the lineation trajectories (inset). Acronyms in and around the BKSK are the same as in Fig. 4. Limits of the Bjerkreim, Sokndal, and Mydland lobes (dashed lines) are as defined in the text.

magnetic lineations are steeply plunging, usually to the south-east, with a calculated mean at N137° SE 68° (Fig. 11b: zone V).

8. Deformation mechanism

Combination of magnetic and field directional data confirms our previous conclusion, mainly based on the S_1 foliation pattern (see Section 4.4), that the L_1/S_1 fabrics are concordant in the whole BKSK stratigraphic series, and, therefore, that the acidic rocks were also affected by the syn-magmatic folding event evidenced in the cumulate series. The now completed L_1/S_1 pattern, summarized by foliation and lineation trajectories on Figs. 9 and 10, gives a comprehensive record of the magmatic to solid-state flow patterns: the lineations point to a convergent flow from the limbs of the three BKSK lobes towards their respective hinge zones, and finally towards a central zone where the flow was steeply plunging. This central zone, which is also outlined by the deflection of the foliation trajectories, is located at the junction between the three lobes, and consists of a funnel-shaped trough that formed in-between the three anorthosite plutons.

The BKSK syncline shape and its L_1/S_1 pattern seem therefore to be strongly controlled by the shape of the neighbouring anorthosite plutons. The emplacement mechanism proposed on petrological grounds for these plutons includes accumulation of a plagioclase mush at the roof of a magma chamber at the base of the crust (~40 km), from which plagioclase-rich masses separate and rise diapirically through the lower crust up to the final level of emplacement (~20 km) (Duchesne et al., 1985; Duchesne and Maquil, 1987). This model, now widely accepted for the anorthosite formation (Ashwal, 1993), has been confirmed by a finite-element modelling (Barnichon et al., 1999). Since the final emplacement of the Egersund–Ogna, Håland–Helleren and Åna–Sira anorthosite plutons is concomitant with the crystallization of the BKSK, with ages around 930 Ma (Schärer et al., 1996), the BKSK syn-magmatic folding is thus readily explained by gravity instability generated by the final emplacement of the anorthosite diapirs. This model accounts for the structural patterns evidenced in the BKSK: sub-vertical foliations wrapping around the contact with neighbouring diapiric plutons, and convergent lineations towards a trough where they become sub-vertical. Such patterns are typical of troughs subsiding by gravity, as pre-

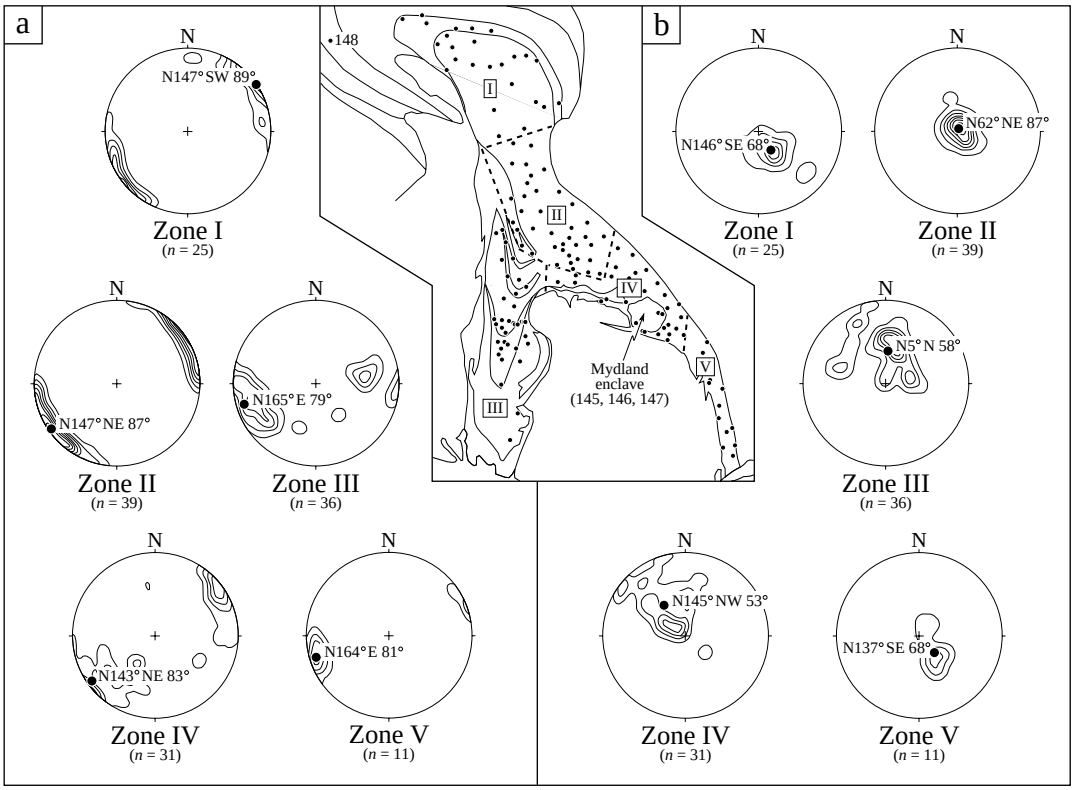

Fig. 11. Schmidt stereo-plots (lower hemisphere) of (a) the magnetic foliations and (b) the magnetic lineations. Each stereo-plot corresponds to a portion of the studied area and is accompanied by the calculated mean magnetic foliation (or lineation) and the number of measurements (n). Zone I = core of the Bjerkreim lobe (i.e. excluding the westernmost AMS sample 148), zone II = central zone, zone III = Sokndal lobe, zone IV = Mydland lobe (around the Mydland enclave, i.e. excluding AMS samples 145, 146, 147), and zone V = Apophysis (south of the Mydland enclave). Limits of the Bjerkreim, Sokndal, and Mydland lobes (dashed lines) are as defined in the text (see also Figs. 9 and 10).

dicted in analogue models of sinking dense layers through a substrate (e.g. Dixon and Summers, 1983), or found in nature, such as in dome-and-basin greenstone/gneiss complexes (Bouhallier et al., 1995; Collins et al., 1998). The three BKSK lobes are therefore adequately described as rim-synclines that developed along the neighbouring anorthosite diapirs. Such rim-syncline structures, resulting from downward flow of material along the flanks of rising diapirs, are predicted by diapir emplacement models (Weinberg and Podladchikov, 1995; Barnichon et al., 1999).

Our conclusion amplifies the gravity-induced subsidence model proposed by Paludan et al. (1994) for the Bjerkreim lobe. These authors mainly based their model on the asymmetrical convergent L_1 path defined in the anorthosite–norite cumulates, which suggests the existence of a subsidence zone in the south-eastern end of the lobe. They also noted that the observed gradation, from pure L-tectonites in the upper part of the hinge zone to L/S-tectonites along the limbs, resembles the pattern produced by the gravitationally subsiding trough modelling of Dixon and Summers (1983). To explain the BKSK folding, Paludan et al. (1994) invoked, however, a possible regional compressive stress field, external to the Rogaland igneous complex, in addition to gravity instabilities. This explanation was in agreement with the views of Michot (1960) and Hermans et al. (1975), who related the BKSK deformation to a folding event with vertical axial planes affecting the granulitic country rocks. However, accepting that the emplacement of the Rogaland igneous complex post-dates the last recorded pervasive regional deformation event by at least 50 My (Schärer et al., 1996; Falkum, 1998), we suggest that the driving force of the BKSK deformation was only gravity. In that understanding, the fabrics in the granulitic gneisses parallel to those of the BKSK would result from transposition of pre-existing structures in the country rocks during emplacement of the complex (Falkum, 1998).

In the general framework of gravity-induced tectonics, the shearing along the Rogaland igneous complex eastern side, responsible for the structures observed in the Apophysis and its north-western extension (see above, Section 4.4), is attributed to accommodation of movements between the eastern border and country rocks (Bolle et al., 1997). Hence, outside the influence of the BKSK subsidence, this sub-vertical shearing can account for the observed steep foliations and lineations.

In the present state of knowledge on the detailed structural and geochronological evolution of South Norway, it is nevertheless premature to definitely preclude the influence of any regional, externally controlled deformation, during the initiation of the emplacement process of the igneous complex. A zone of crustal weakness may have channelled the diapiric uprise of the anorthosite plutons (Duchesne et al., 1999).

9. Summary and conclusions

The magnetic fabric survey, which focuses on the massive acidic upper part of the BKSK, provides evidence that, although highly petrographically variable, the rocks' magnetic susceptibility and AMS are mainly controlled by magnetite. Field observations and image analysis verify the principle of coaxiality between magnetic fabric and petrofabric. Hence, both fabrics can be combined to picture the internal structure of the BKSK. The observed L/S patterns demonstrate that the influx and crystallization of successive magma pulses took place in a magma chamber that was simultaneously deforming by subsidence of its floor. It is proposed that this sinking was gravity-induced, in connection with the final stage of diapiric emplacement of the neighbouring anorthosite plutons. The convergent flow towards a central trough, where all the lineations become steep, constitutes a major argument in favour of a gravity-driven process. The BKSK is therefore viewed as a composite rim-syncline, which developed by downward return flow of material along rising anorthosite plutons. It is further suggested that the BKSK subsidence was coeval with the development of a gravity induced accommodation zone along the eastern border of the Rogaland igneous complex. This accommodation zone would have favoured emplacement of the Apophysis material and intrusion of the BKSK acidic magma across the Mydland lobe cumulates. Gravity-induced tectonics can account for the observed structures, but it is not possible to rule out completely the simultaneous influence of a weak externally driven stress field.

Acknowledgements

The Belgian Fund for Joint Basic Research provided financial support for fieldwork. B. Hoffer and S. Genin are thanked for their help in the field. A thorough review by J. L. Bouchez and suggestions by P. Launeau were greatly appreciated. C. Walter revised the English. Comments from two anonymous reviewers of the Journal of Structural Geology were very stimulating.

References

Archanjo, C.J., Macedo, J.W.P., Galindo, A.C., Araùjo, M.G.S., 1998. Brasiliano crustal extension and emplacement fabrics of the

mangerite–charnockite pluton of Umarizal, north-east Brazil. Precambrian Research 87, 19–32.

Ashwal, L., 1993. Anorthosites. Springer-Verlag, Berlin.

Barnichon, J.D., Havenith, H., Hoffer, B., Charlier, R., Jongmans, D., Duchesne, J.C., 1999. The deformation of the Egersund–Ogna anorthosite massif, south Norway: finite-element modelling of diapirism. Tectonophysics 303, 109–130.

Bingen, B., van Breemen, O., 1998. U–Pb monazite ages in amphibolite- to granulite-facies orthogneiss reflect hydrous mineral breakdown reactions: Sveconorwegian Province of SW Norway. Contributions to Mineralogy and Petrology 132, 336–353.

Bolle, O. 1996. L'Apophyse du massif stratiforme de Bjerkreim–Sokndal (Rogaland, Norvège): une intrusion composite de la suite charnockitique. In: Demaiffe, D. (Ed.), Petrology and Geochemistry of Magmatic Suites of Rocks in the Continental and Oceanic Crusts. ULB-MRAC, Bruxelles, pp. 129–144.

Bolle, O., 1998. Mélanges magmatiques et tectonique gravitaire dans l'Apophyse de l'intrusion de Bjerkreim–Sokndal (Rogaland, Norvège): pétrologie, géochimie et fabrique magnétique. Ph.D. thesis, Université de Liège.

Bolle, O., Diot, H., Duchesne, J.C., 1997. Anisotropie de la susceptibilité magnétique dans une intrusion composite de la suite charnockitique: l'apophyse du massif stratiforme de Bjerkreim–Sokndal (Rogaland, Norvège méridionale). Comptes Rendus de l'Académie des Sciences de Paris (Série IIa) 325, 799–805.

Borradaile, G.J., Henry, B., 1997. Tectonic applications of magnetic susceptibility and its anisotropy. Earth-Science Reviews 42, 49–93.

Bouchez, J.L. 1997. Granite is never isotropic: an introduction to AMS studies of granitic rocks. In: Bouchez, J.L., Hutton, D.H.W., Stephens, W.E. (Eds.), Granite: From Segregation of Melts to Emplacement Fabrics. Kluwer, Dordrecht, pp. 95–112.

Bouhallier, H., Chardon, D., Choukroune, P., 1995. Strain patterns in Archaean dome-and-basin structures: The Dharwar craton (Karnataka, South India). Earth and Planetary Science Letters 135, 57–75.

Clark, D.A., 1997. Magnetic petrophysics and magnetic petrology: aids to geological interpretation of magnetic surveys. Journal of Australian Geology and Geophysics 17, 83–103.

Collins, W.J., van Kranendonk, M.J., Teyssier, C., 1998. Partial convective overturn of Archean crust in the east Pilbara Craton, Western Australia: driving mechanisms and tectonic implications. Journal of Structural Geology 20, 1405–1424.

Demaiffe, D., 1972. Etude pétrologique de l'Apophyse Sud-Est du massif de Bjerkrem–Sogndal (Norvège méridionale). Annales de la Société Géologique de Belgique 95, 255–269.

Demaiffe, D., 1977. De l'origine des anorthosites. Pétrologie, géochimie et géochimie isotopique des massifs anorthositiques de Hidra et Garsaknatt (Rogaland, Norvège méridionale). Ph.D. thesis, Université Libre de Bruxelles.

Demaiffe, D., Duchesne, J.C., Michot, J., Pasteels, P., 1973. Le massif anorthosito-leuconoritique d'Hidra et son faciès de bordure. Comptes Rendus de l'Académie des Sciences de Paris (Série D) 227, 17–20.

Dixon, J.M., Summers, J.M., 1983. Patterns of total and incremental strain in subsiding troughs: experimental centrifuge models of inter-diapir synclines. Canadian Journal of Earth Sciences 20, 1843–1861.

Duchesne, J.C., 1972. Fe–Ti oxide minerals in the Bjerkrem–Sogndal massif, South-western Norway. Journal of Petrology 13, 57–81.

Duchesne, J.C. 1996. Liquid ilmenite or liquidus ilmenite: a comment on the nature of ilmenite vein deposits. In: Demaiffe, D. (Ed.), Petrology and Geochemistry of Magmatic Suites of Rocks in the Continental and Oceanic Crusts. ULB-MRAC, Bruxelles, pp. 73–81.

Duchesne, J.C., Liégeois, J.P., Vander Auwera, J., Longhi, J., 1999. The crustal tongue melting model and the origin of massive anorthosites. Terra Nova 11, 100–105.

Duchesne, J.C., Maquil, R., 1987. The Egersund–Ogna massif. In: Maijer, C., Padget, P. (Eds.), The Geology of Southernmost Norway, Norges Geologiske Undersøkelse Special Publication, 1, pp. 50–56.

Duchesne, J.C., Maquil, R., Demaiffe, D. 1985. The Rogaland anorthosites: facts and speculations. In: Tobi, A., Touret, J.L.R. (Eds.), The Deep Proterozoic Crust in the North Atlantic Provinces. Riedel, Dordrecht, pp. 449–476.

Duchesne, J.C., Wilmart, E., 1997. Igneous charnockites and related rocks from the Bjerkreim–Sokndal layered intrusion (Southwest Norway): a jotunite (hypersthene monzondiorite)-derived A-type granitoid suite. Journal of Petrology 387, 337–369.

Duchesne, J.C., Wilmart, E., Demaiffe, D., Hertogen, J., 1989. Monzonorites from Rogaland (Southwest Norway): a series of rocks coeval but not comagmatic with massif-type anorthosites. Precambrian Research 7, 111–128.

Falkum, T., 1982. Geologisk kart over Norge, berggrunnskart Mandal. Norges Geologiske Undersøkelse Map, scale 1:250,000.

Falkum, T., 1998. The Sveconorwegian magmatic and tectonometamorphic evolution of the high-grade Proterozoic Flekkefjord complex, South Norway. Norges Geologiske Undersøkelse Bulletin 434, 5–33.

Falkum, T., Petersen, J.S., 1980. The Sveconorwegian orogenic belt, a case of Late-Proterozoic plate-collision. Geologische Rundschau 69, 622–647.

Ferré, E., Gleizes, G., Djouadi, M.T., Bouchez, J.L., Ugodulunwa, F.X.O. 1997. Drainage and emplacement of magmas along an inclined transcurrent shear zone: petrophysical evidence from a granite–charnockite pluton (Rahama, Nigeria). In: Bouchez, J.L., Hutton, D.H.W., Stephens, W.E. (Eds.), Granite: From Segregation of Melts to Emplacement Fabrics. Kluwer, Dordrecht, pp. 253–273.

Flinn, D., 1965. On the symmetry principle and the deformation ellipsoid. Geological Magazine 102, 36–45.

Gapais, D., 1989. Shear structures within deformed granites: mechanical and thermal indicators. Geology 17, 1144–1147.

Grégoire, V., Darrozes, J., Gaillot, P., Nédélec, A., Launeau, P., 1998. Magnetite grain shape fabric and distribution anisotropy versus magnetic fabric: a 3D-case study. Journal of Structural Geology 20, 937–944.

Hargraves, R.B., Johnson, D., Chan, C.W., 1991. Distribution anisotropy: the cause of AMS in igneous rocks? Geophysical Research Letters 18, 2193–2196.

Hermans, G.A.E.M., Tobi, A.C., Poorter, R.P.E., Maijer, C., 1975. The high-grade metamorphic Precambrian of the Sirdal–Ørsdal area, Rogaland/Vest-Agder, southwest Norway. Norges Geologiske Undersøkelse Bulletin 318, 51–74.

Holland, T.J.B., Babu, E.V.S.S.K., Waters, D.J., 1996. Phase relations of osumilite and dehydration melting in pelitic rocks: a simple thermodynamic model for the KFMASH system. Contributions to Mineralogy and Petrology 124, 383–394.

Irvine, T.N. 1987. Layering and related structures in the Duke Island and Skaergaard intrusions: similarities, differences and origins. In: Parsons, I. (Ed.), Origins of Igneous Layering. Riedel, Dordrecht, pp. 185–245.

Jelinek, V., 1981. Characterization of the magnetic fabrics of rocks. Tectonophysics 79, T63–T67.

Jover, O., Rochette, P., Lorand, J.P., Maeder, M., Bouchez, J.L., 1989. Magnetic mineralogy of some granites from the French Massif Central: origin of their low-field susceptibility. Physics of the Earth and Planetary Interiors 55, 79–92.

Krause, H., Gierth, E., Schott, W., 1985. Ti–Fe deposits in the South Rogaland igneous complex with special reference to the Åna–Sira anorthosite massif. Norges Geologiske Undersøkelse Bulletin 402, 25–37.

Krause, H., Pedall, K.G., 1980. Fe–Ti mineralizations in the Åna–Sira anorthosite, Southern Norway. In: Siivola, J. (Ed.), Metallogeny of the Baltic Shield, Geological Survey of Finland Special Publication, 307, pp. 56–83.

Launeau, P., Cruden, A.R., 1998. Magmatic fabric mechanisms in a syenite: results of a combined anisotropy of magnetic susceptibility and image analysis study. Journal of Geophysical Research — Solid Earth 103, 5067–5089.

Launeau, P., Robin, P.Y.F., 1996. Fabric analysis using the intercept method. Tectonophysics 267, 91–119.

Maijer, C., 1987. The metamorphic envelope of the Rogaland intrusive complex. In: Maijer, C., Padget, P. (Eds.), The Geology of Southernmost Norway, Norges Geologiske Undersøkelse Special Publication, 1, pp. 68–73.

Michot, J., 1961. The anorthositic complex of Haaland–Helleren. Norsk Geologisk Tidsskrift 41, 157–172.

Michot, J., Michot, P., 1969. The problem of the anorthosites. The South-Rogaland igneous complex (Southwestern Norway). In: Isachsen, Y.W. (Ed.), Origin of the Anorthosites and Related Rocks, New York State Museum Science Service Memoir, 18, pp. 399–410.

Michot, P., 1960. La géologie de la catazone, le problème des anorthosites, la palingenèse basique et la tectonique catazonale dans le Rogaland méridional (Norvège méridionale). Norges Geologiske Undersøkelse Bulletin 212, 1–54.

Nielsen, F.M., Campbell, I.H., McCulloch, M., Wilson, J.R., 1996. A strontium isotopic investigation of the Bjerkreim–Sokndal layered intrusion, Southwest Norway. Journal of Petrology 37, 171–193.

Nielsen, F.M., Wilson, J.R., 1991. Crystallization processes in the Bjerkreim–Sokndal layered intrusion, south Norway: evidence from the boundary between two macrocyclic units. Contributions to Mineralogy and Petrology 107, 403–414.

Paludan, J., Hansen, U.B., Olesen, N.Ø, 1994. Structural evolution of the Precambrian Bjerkreim–Sokndal intrusion, South Norway. Norsk Geologisk Tidsskrift 74, 185–198.

Paterson, S.R., Vernon, R.H., Tobisch, O.T., 1989. A review of criteria for the identification of magmatic and tectonic foliations in granitoids. Journal of Structural Geology 11, 349–363.

Rietmeijer, F.J.M., 1979. Pyroxenes from iron-rich igneous rocks in Rogaland, SW Norway. Geologica Ultraiectina 21.

Rochette, P., 1987. Magnetic susceptibility of the rock matrix related to magnetic fabric studies. Journal of Structural Geology 9, 1015–1020.

Rochette, P., Aubourg, C., Perrin, M., 1999. Is this magnetic fabric normal? A review and case studies in volcanic formations. Tectonophysics 307, 219–234.

Rochette, P., Jackson, M., Aubourg, C., 1992. Rock magnetism and the interpretation of anisotropy of magnetic susceptibility. Reviews of Geophysics 30, 209–226.

Saint Blanquat (de), M., Tikoff, B. 1997. Development of magmatic to solid-state fabrics during syntectonic emplacement of the Mono Creek granite, Sierra Nevada batholith. In: Bouchez, J.L., Hutton, D.H.W., Stephens, W.E. (Eds.), Granite: From Segregation of Melts to Emplacement Fabrics. Kluwer, Dordrecht, pp. 231–252.

Schärer, U., Wilmart, E., Duchesne, J.C., 1996. The short duration and anorogenic character of anorthosite magmatism: U–Pb dating of the Rogaland complex, Norway. Earth and Planetary Science Letters 139, 335–350.

Shimamoto, T., Ikeda, Y., 1976. A simple algebraic method for strain estimation from deformed ellipsoidal objects. 1. Basic theory. Tectonophysics 36, 315–337.

Streckeisen, A., 1974. How should charnockitic rocks be named? In: Bellière, J., Duchesne, J.C. (Eds.), Géologie des domaines cristallins. Volume du centenaire de la Société Géologique de Belgique, pp. 349–360.

Uyeda, S., Fuller, M.D., Belshe, J.C., Girdler, R.W., 1963. Anisotropy of magnetic susceptibility of rocks and minerals. Journal of Geophysical Research 68, 279–291.

Vander Auwera, J., Longhi, J., 1994. Experimental study of a jotunite (hypersthene monzodiorite): constraints on the parent magma composition and crystallization conditions (P, T, fO_2) of the Bjerkreim–Sokndal intrusion (Norway). Contributions to Mineralogy and Petrology 118, 60–78.

Van der Plas, L., Tobi, A.C., 1965. A chart for judging the reliability of point counting results. American Journal of Science 263, 87–90.

Weinberg, R.F., Podladchikov, Y.Y., 1995. The rise of solid-state diapirs. Journal of Structural Geology 17, 1183–1195.

Wiebe, R.A., 1984. Co-mingling of magmas in the Bjerkrem–Sogndal lopolith (southwest Norway): evidence for the compositions of residual liquids. Lithos 17, 171–188.

Wilmart, E., Duchesne, J.C., 1987. Geothermobarometry of igneous and metamorphic rocks around the Åna–Sira anorthosite massif: implications for the depth of emplacement of the South Norwegian anorthosites. Norsk Geologisk Tidsskrift 67, 185–196.

Wilson, J.R., Robins, B., Nielsen, F.M., Duchesne, J.C., Vander Auwera, J. 1996. The Bjerkreim–Sokndal layered intrusion, Southwest Norway. In: Cawthorn, R.G. (Ed.), Layered Intrusions. Elsevier, Amsterdam, pp. 231–255.